Local Glutamate-Glutamine Cycling Underlies Presynaptic ATP Homeostasis

Reinoud Maex[1]

[1]Biocomputation Research Group, University of Hertfordshire, UK.

Keywords: analytical model, bioenergetics, axon, astrocyte, neurotransmitter, tricarboxylic acid cycle

Abstract

Presynaptic axon terminals maintain in their cytosol an almost constant level of adenosine triphosphate (ATP) to safeguard neurotransmission during varying workloads. In the present study, it is argued that the vesicular release of neurotransmitter, and the recycling of transmitter via astrocytes, may itself be a mechanism of ATP homeostasis. In a minimal metabolic model of a presynaptic axon bouton, the accumulation of glutamate into vesicles and the activity-dependent supply of its precursor glutamine by astrocytes

generated a steady-state level of ATP that was independent of the workload. When the workload increased, an enhanced supply of glutamine raised the rate of ATP production through the conversion of glutamate to the Krebs cycle intermediate α-ketoglutarate. The accumulation and release of glutamate, on the other hand, acted as a leak that diminished ATP production when the workload decreased. The fraction of ATP which the axon spent on the release and recycling of glutamate was small (4.7 %), irrespective of the workload. Increasing this fraction enhanced the speed of ATP homeostasis, and reduced the futile production of ATP. The model can be extended to axons releasing other, or coreleasing multiple, transmitters. Hence, the activity-dependent formation and release of neurotransmitter may be a universal mechanism of ATP homeostasis.

1 Introduction

According to the law of mass action, the rate at which energy is retrieved from the oxidation of glucose can be enhanced by increasing the supply of glucose and oxygen, by enhancing the concentration of catalysts, or by accelerating the disposal of the reaction products (Segel, 1984). A swift disposal of the reaction products (CO_2 and H_2O in case of complete oxidation) is so important that it can be expedient, for the fast retrieval of energy, to release to the environment incompletely oxidized intermediates such as lactate.

Neurons are cells specialized in the disposal of neurotransmitter. It is therefore legitimate to ask if they can use transmitter release to regulate their own rate of glucose consumption (and the concomitant production of the high-potential intermedi-

ary adenosine triphosphate, ATP), even if at face value neurotransmitter release is an energy-consuming process (Attwell & Laughlin, 2001).

Presynaptic axon boutons maintain in their cytosol an ATP concentration of about 1.5 mM (Erecińska & Silver, 1989; Rangaraju, Calloway, & Ryan, 2014), in spite of fluctuations in the workload and the lack of substantial energy stores. Most of the ATP is synthesized in the mitochondria (Dienel, 2019; Hall, Klein-Flügge, Howarth, & Attwell, 2012), which are present in 47 % of the varicosities along hippocampal Schaffer collaterals (Shepherd & Harris, 1998). A small part of the ATP production ($<$ 10 %, Attwell & Laughlin, 2001; Yu, Herman, Rothman, Agarwal, & Hyder, 2018) is spent on the vesicular accumulation, release and recycling of neurotransmitter, which in cerebral cortex is L-glutamate (Glu) for 85 % of the synapses (Beaulieu & Colonnier, 1985).

Astrocytes, extensions of which enwrap the synapses (Ghézali, Dallérac, & Rouach, 2016), take up the Glu released in the synaptic cleft, and convert it to L-glutamine (Gln) (see for review Andersen et al., 2021; Dienel, 2019; Hertz, 2004; Marx, Billups, & Billups, 2015). Glutamine is in turn released from the astrocyte through connexin 43 hemichannels (Cheung et al., 2022), and enters via a Na^+-dependent transporter the presynaptic axon bouton, where it is hydrolyzed to Glu, thus completing the Glu-Gln cycle (see Figure A1 in appendix A).

In the presynaptic bouton, the newly formed Glu can replenish the cytosolic pool of neurotransmitter (Hertz, 2004), or it can be inserted into the mitochondrial Krebs cycle after conversion to α-ketoglutarate (αKG). The concentration of αKG and other Krebs cycle intermediates determines the cycle's capacity to oxidize its substrate acetyl-CoA

and to produce ATP (Dienel, 2019; Nelson & Cox, 2013). It was the observation by Szent-Gyorgyi that these intermediate compounds, when added to a muscle preparation, enhanced the oxygen consumption by a factor far beyond that needed for their own oxidation, hence that they acted as catalysts, that led Krebs to postulate his eponymous cycle (Krebs, 1953).

Mitochondrial physiology is complex, with energy being stored in the phosphorylation potential $\frac{[\mathrm{ATP}]}{[\mathrm{ADP}]\ [\mathrm{P_i}]}$ (the ratio of ATP to its hydrolysis products adenosine diphosphate and inorganic phosphate[1]), in the (inverse redox) potential $\frac{[\mathrm{NADH}]}{[\mathrm{NAD^+}]}$ (the ratio of reduced to oxidized nicotinamide-adenine dinucleotide), and in the electrical and proton gradients across the inner membrane. Although the chain of energy transductions, and the associated transport processes, are well described (Nicholls & Ferguson, 2002), it is still unknown how the metabolic pathways are recruited that provide the energy to drive ATP synthesis (for neurons: the lysis of glucose in the cytosol, followed by the oxidation of pyruvate in the mitochondria). Proposed mechanisms are mass action by ATP, ADP, $\mathrm{P_i}$ and the coenzymes $\mathrm{NAD^+}$ and NADH (Brown, 1992; Krebs, 1970), positive and negative allosteric modulation of enzymes by the same compounds (Nelson & Cox, 2013), and the activation of mitochondrial dehydrogenases by $\mathrm{Ca^{2+}}$ ions

[1] This kinetic expression is commonly used instead of the Gibbs potential $RT \ln \left[\frac{[\mathrm{ATP}]}{[\mathrm{ATP}]^{\mathrm{e}}} \frac{[\mathrm{ADP}]^{\mathrm{e}}}{[\mathrm{ADP}]} \frac{[\mathrm{P_i}]^{\mathrm{e}}}{[\mathrm{P_i}]} \right]$ (the superscript denoting the concentrations at equilibrium). Note that each concentration represents collectively all different ionization states of its species, including the complexes with cations. Hence these expressions are only valid at constant pH and $[\mathrm{Mg^{2+}}]$, in which case the fractions of ionized and complexed species are constant (Alberty, 1969).

(Cortassa, Aon, Marbán, Winslow, & O'Rourke, 2003; Denton & McCormack, 1980).

Here it is proposed that axon boutons, by importing Gln and releasing Glu, adapt the capacity of their mitochondrial Krebs cycle to varying workloads. An analytical model was built to elaborate this hypothesis.

2 A minimal model of a presynaptic axon compartment

Section 2.1 introduces the constituent biochemical reactions of the model, which is then reduced, in section 2.2, to two differential equations of the axon's cytosolic concentrations of ATP and Glu. The values of the free parameters are determined in sections 2.3 and 2.4, with section 2.5 adding two variants of the model to be used as controls.

2.1 Functional description of the model in terms of its constituent biochemical reactions

Figure 1 depicts the relevant reactions involving Glu and ATP in a presynaptic axon bouton. A detailed description, with references, is provided in appendix B.

- The axon bouton continually replenishes its pool of Glu by importing Gln from the perisynaptic astrocyte. The Gln is converted to Glu by a phosphate-activated glutaminase (PAG) located on the outer surface of the inner mitochondrial membrane (see appendix section B.1).

- Within the mitochondrial matrix, changes in the concentration of Glu are rapidly balanced by changes in the concentration of the Krebs cycle intermediate αKG. In

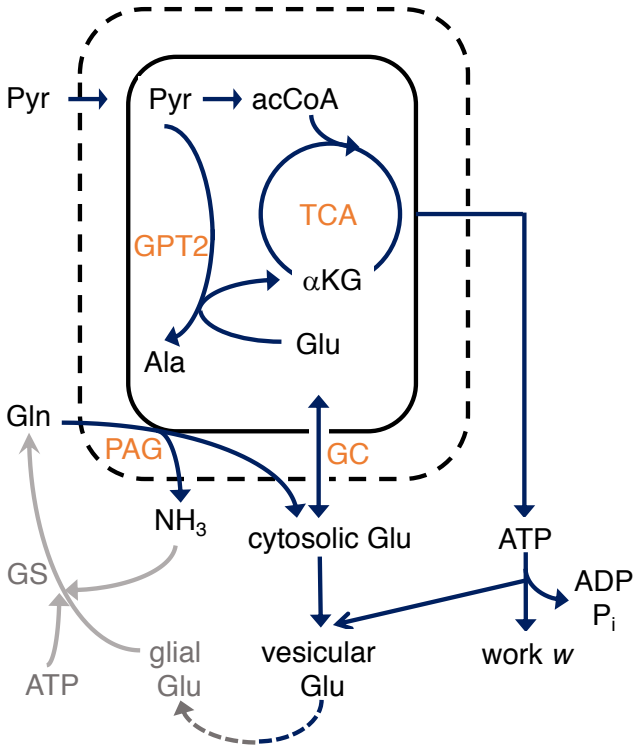

Figure 1: Reaction diagram of glutamate and ATP in a presynaptic axon compartment. The dashed and solid contours represent the outer and inner mitochondrial membrane. For a detailed description, please see text of section 2.1 and appendix B. Pathways in gray take place in the perisynaptic astrocyte and were not explicitly modeled. Abbreviations: acCoA, acetyl-coenzyme A; ADP, adenosine diphosphate; αKG, α-ketoglutarate; Ala, alanine; ATP, adenosine triphosphate; GC, glutamic acid carrier; Gln, glutamine; Glu, glutamate; GPT2, mitochondrial glutamate-pyruvate aminotransferase; GS, glutamine synthase; P_i, inorganic phosphate; PAG, P_i-activated glutaminase; Pyr, pyruvate; TCA, tricarboxylic acid (or Krebs) cycle; w, workload.

the model this interconversion is catalysed by a glutamate-pyruvate aminotransferase (GPT2), although other enzymes such as Glu dehydrogenase may participate as well (appendix section B.2).

- Cytosolic Glu is exchanged for mitochondrial Glu via a bidirectional glutamic acid carrier (GC) located in the inner mitochondrial membrane (appendix section B.3).

- Cytosolic Glu is accumulated in synaptic vesicles at a rate dependent on its own concentration and that of ATP (appendix section B.4).

Of these four reactions, the first (Glu formation by the PAG enzyme) and last (disposal of Glu through accumulation in vesicles) are *de facto* irreversible. During a constant workload, their rates will be shown to scale with the workload. In contrast, the transamination of Glu by GPT2 and the transport of Glu through the GC carrier are reversible reactions, but they proceed only, in one or the other direction, when a change in the cytosolic Glu level signals a change in workload.

2.2 Mathematical formulation of the model

2.2.1 Equations and symbols

The reaction scheme of Figure 1 was reduced to two differential equations describing the variation over time t of the cytosolic concentrations of L-glutamate, [Glu], and

adenosine triphosphate, [ATP], in response to a change of the workload w:

$$\frac{\mathrm{d}\,[\mathrm{Glu}]}{\mathrm{d}t} = \omega \underbrace{\kappa_1\,[\mathrm{Gln}]\,[\mathrm{P_i}]^2}_{\text{formation by PAG}} - \underbrace{\kappa_2\,[\mathrm{Glu}]\,[\mathrm{ATP}]}_{\text{vesicular accumulation}} \tag{1}$$

$$\frac{\mathrm{d}\,[\mathrm{ATP}]}{\mathrm{d}t} = \underbrace{\kappa_3\,[\mathrm{Glu}]\,[\mathrm{Pyr}]\left[\frac{[\mathrm{P_i}]\,[\mathrm{ADP}]}{[\mathrm{ATP}]}\right]}_{\text{production in mitochondria}} - \underbrace{\frac{\kappa_2}{2}\,[\mathrm{Glu}]\,[\mathrm{ATP}]}_{\text{vesicle acidification}} - \underbrace{w\,[\mathrm{ATP}]}_{\text{work}} - \omega\,\underbrace{\kappa_1\,[\mathrm{Gln}]\,[\mathrm{P_i}]^2}_{\text{Gln import}}. \tag{2}$$

The third dependent variable, the concentration of inorganic phosphate, $[\mathrm{P_i}]$, is a static function of [ATP],

$$[\mathrm{P_i}] = 0.2([\mathrm{ATP}]_{\max} - [\mathrm{ATP}]), \tag{3}$$

where $[\mathrm{ATP}]_{\max}$ was put to 9 mM to allow ATP to reach levels > 8 mM, as have been obtained in experiments in which the exocytosis of vesicles was eliminated (Rangaraju et al., 2014, experiments to be simulated in section 3.5).

The independent variable w denotes collectively all ATP-consuming processes, except those directly involved in the formation and vesicular accumulation of Glu. In a presynaptic axon terminal, w would chiefly consist of electrochemical processes such as the pumping of Na^+ and Ca^{2+} out of the cell (Attwell & Laughlin, 2001).

The symbol ω is a hyperparameter, whose default value is taken proportional to the workload w (see Table 1 for the default values of this and other symbols). The biophysical processes justifying such a covariation between ω and w are discussed in section 4.1.

Table 1: Variables and Parameters of the Model of Equations 1 and 2

Symbol	Physical Quantity	Nature	Default Value
$[\mathrm{Glu}]$	cytosolic concentration of L-glutamate	variable	1.0 mM [a]
$[\mathrm{ATP}]$	cytosolic concentration of adenosine triphosphate	variable	1.5 mM [b,c]
$[\mathrm{P_i}]$	cytosolic concentration of inorganic phosphate	variable	1.5 mM [c]
w	workload	independent variable	$1.0\ \mathrm{s}^{-1}$
$[\mathrm{Gln}]$	cytosolic concentration of L-glutamine	constant	0.4 mM [d]
$[\mathrm{Pyr}]$	mitochondrial concentration of L-pyruvate	constant	0.04 mM [e]
κ_1	rate constant of Glu formation	parameter	$1/18.3\ \mathrm{mM}^{-2}\ \mathrm{s}^{-1}$
κ_2	rate constant of vesicular Glu accumulation	parameter	$1/30.5\ \mathrm{mM}^{-1}\ \mathrm{s}^{-1}$
κ_3	rate constant of mitochondrial ATP production	parameter	$800/30.5\ \mathrm{mM}^{-2}\ \mathrm{s}^{-1}$
ω	activity-dependence of Glu formation	hyperparameter	$w \times (1\ \mathrm{s})$

[a] Lower end of physiological range in Ishikawa, Sahara, and Takahashi (2002).

[b] Rangaraju et al. (2014).

[c] Erecińska and Silver (1989).

[d] Two to three times lower than [Glu] (Erecińska & Silver, 1990, p. 250).

[e] Arce-Molina et al. (2020).

2.2.2 Dynamics of the cytosolic glutamate concentration

The first term of equation 1 shows that Glu is synthesized by the PAG enzyme at a rate proportional to the concentration of its precursor Gln and to the square of the concentration of the positive allosteric modulator P_i (Kvamme, Torgner, & Roberg, 2001; Tveit, Svenneby, & Kvamme, 1970). Glutamine being a 'storage form of glutamate' (Cooper & Jeitner, 2016), its concentration was taken constant at 0.4 mM (Westergaard, Waagepetersen, Belhage, & Schousboe, 2017). This constant could evidently have been absorbed in the free parameter κ_1, but is written out for clarity.

Glutamate is disposed of into a virtual pool of synaptic vesicles (second term of equation 1). Thus, Glu is removed from the cytosol at a rate proportional to both [Glu] and [ATP] (Budzinski, Zeigler, Fujimoto, Bajjalieh, & Chiu, 2011; Schuldiner, Shirvan, & Linial, 1995). The filling of actual vesicles is pH-dependent, but with vesicles reacidifying and refilling with a time-constant of about 15 s (Egashira, Takase, & Takamori, 2015; Hori & Takahashi, 2012) and being released at a baseline rate of 1 Hz (Attwell & Laughlin, 2001), a sufficient number of vesicles was assumed to be available, in different stages of refilling, to average out this pH-dependency, which is now contained in parameter κ_2. The proton gradient generated by one ATP molecule suffices to transport ≈ 2 Glu molecules (Egashira et al., 2015; Johnson, Beers, & Scarpa, 1982), hence the presence of a stoichiometric factor 0.5 in the corresponding term of equation 2. The effect of varying κ_2 is examined in section 3.3.

2.2.3 Dynamics of the cytosolic ATP concentration

The *ad hoc* model of axonal ATP production (first term of equation 2) assumes that, under physiological conditions, the mitochondrial Krebs cycle is the rate-limiting process in the oxidation of glucose, and that upstream glycolysis and downstream respiration rapidly adapt their flow to that of the Krebs cycle. Upstream glycolysis can, in principle, generate ATP 100 times faster (so long as glucose is supplied and lactate disposed of, see Vaupel & Multhoff, 2021), and the enzymes of the Krebs cycle and the protein complexes of the respiratory chain (mediating NADH-driven proton pumping, proton-driven ATP synthesis, and the expulsion of ATP into the cytosol via the ATP^{4-}/ADP^{3-} translocator) are assumed to be present in sufficient numbers not to be rate-limiting (Garcia, Gupta, Bartol, Sejnowski, & Rangamani, 2023). What *is* rate-limiting then is the mitochondrial concentration of oxaloacetate, the compound that fuses with acetyl-CoA to form citrate (Krebs, 1970). In one turn of the Krebs cycle, the citrate forms a new oxaloacetate molecule after the complete oxidation of an acetyl moiety. Crucially, neurons have only a very limited capacity to form oxaloacetate from pyruvate, and they rely on the import of Gln from astrocytes to replenish, if needed, their pool of Krebs cycle intermediates (see panel B of appendix Figure A1) (Dienel, 2019; Hertz, Dringen, Schousboe, & Robinson, 1999).

In the first term of equation 2, then, [Glu] represents the capacity of the Krebs cycle. Cytosolic [Glu] is used as a surrogate for the mitochondrial concentration of αKG, and by extension for the size of the entire pool of Krebs cycle intermediates (see appendix sections B.2 and B.3). The substitution of $[\text{Glu}]_\text{c}$ for $[\alpha\text{KG}]_\text{m}$ requires that the two reactions in Figure 1 that interconvert Glu and αKG (the transport of Glu via the GC

carrier and its transamination by GPT2) are fast enough to be at quasi-steady state.

The second factor is the mitochondrial concentration of the substrate of the Krebs cycle, acetyl-CoA, here represented by its precursor pyruvate (Pyr), the concentration of which was taken constant at 40 μM (Arce-Molina et al., 2020). This constancy of [Pyr] reflects the need for neurons to rapidly adjust their rate of glycolysis to that of the Krebs cycle in order to preserve mass balance[2] (Magnus & Keizer, 1997; Mason et al., 1995; Nelson & Cox, 2013). This adaptation involves an array of non-modeled processes, including allosteric modulation of the enzyme phosphofructokinase-1 (positively by ADP, negatively by ATP and citrate, see Nelson & Cox, 2013), and, on a longer time-scale, the mobilization of glucose transporters to the cell membrane (Ashrafi, Wu, Farrell, & Ryan, 2017) and adaptation of the local blood flow (Li & Freeman, 2015).

The third, bracketed, factor is the inverse of the cytosolic phosphorylation potential (see footnote 1), a key regulator of mitochondrial ATP production (Brown, 1992; Erecińska & Dagani, 1990). The processes implicit in this expression can be summarized as follows. An elevated cytosolic ADP level stimulates the exchange of ADP^{3-} for mitochondrial ATP^{4-} via the adenine nucleotide translocator. The resulting increase in $[ADP]_m$, and decrease in $[ATP]_m$, reduces the mitochondrial phosphorylation potential and stimulates ATP production by the ATP synthase, provided the proton gradient does not degrade. The translocation, however, and the associated import of P_i, causes a pro-

[2] Lactate production was assumed to be negligible so that the flux of the Krebs cycle was twice that of glycolysis at steady state. Accordingly, the first term of equation 2 counts the aggregate ATP production of mitochondria and cytosol, hence including the two ATP molecules (out of 32) produced by glycolysis (Dienel, 2019).

ton to enter (Nicholls & Ferguson, 2002), and to restore the proton gradient the flux of the Krebs cycle must increase, which can be achieved by the allosteric effects of ADP_m (+) and ATP_m $(-)$ on the pyruvate dehydrogenase complex and on several enzymes in the first steps of the Krebs cycle (Nelson & Cox, 2013). These allosteric actions operate on a time-scale much faster than that of expanding the Krebs cycle, and they can therefore be assumed to be at quasi-steady state. Advantage can further be taken of the observation that, in creatine-containing cells and under saturating oxygen conditions, the ADP content covaries with $[P_i]$ (Jeneson, Westerhoff, Brown, Van Echteld, & Berger, 1995, their Figures 3 and 5). In this scenario, then, parameter κ_3 contains not only the constant of proportionality between $[P_i]$ and [ADP], but also other constants such as the fraction of ADP_c (ATP_m) that is ionized in the form ADP^{-3} (ATP^{-4}) (Magnus & Keizer, 1997), the value of the NADH potential (Erecińska & Dagani, 1990), and the magnitude of the allosteric effects.

As for the rate of ATP *consumption*, the second term of equation 2 represents the ATP hydrolyzed for the acidification of vesicles (same decay term as in equation 1, taking into account the stoichiometry). The release process itself (exo- and endocytosis of vesicles) was not modeled, but in so far as membrane currents are involved in it, the work done to restore the ion gradients is part of the workload w.

The work term collects all ATP-consuming processes, except the ATP used for vesicle acidification (counted by the second term) and the one for the import of Gln (last term). The workload w may contain terms such as the cytosolic concentrations of Na^+

and Ca^{2+}, which, when elevated, activate the respective ion pumps[3].

The last term of equation 2, labeled 'Gln import', is identical to the first term of equation 1, and counts the single ATP molecule that is needed to restore the Na^+ gradient after the entry of a Gln molecule (Varoqui, Zhu, Yao, Ming, & Erickson, 2000).

2.3 Calibration of the model

After substitution of $[P_i]$ for [ADP] (see section 2.2.3), equations 1 and 2 read at steady state

$$\omega\, \kappa_1\, [\mathrm{Gln}]\, [\mathrm{P_i}]^2 = \kappa_2\, [\mathrm{Glu}]\, [\mathrm{ATP}] \tag{4}$$

$$\kappa_3\, [\mathrm{Glu}]\, [\mathrm{Pyr}]\, [\mathrm{P_i}]^2 = 1.5\, \kappa_2\, [\mathrm{Glu}]\, [\mathrm{ATP}]^2 + w[\mathrm{ATP}]^2. \tag{5}$$

The baseline workload was empirically set to unity (see section 2.4 for a justification). Then, with $w = 1\,\mathrm{s}^{-1}$, the values of parameters κ_{1-3} were determined from equations 4 and 5 using the following three conditions: 1) the baseline level of ATP; 2) the baseline level of Glu; and 3) the presumed fraction of ATP a neuron spends on Glu release and recycling.

Baseline [ATP] was assigned its physiological value of 1.5 mM, implying, from equation 3, that baseline $[P_i]$ = 1.5 mM as well (Erecińska & Silver, 1989; Rangaraju et

[3] This work term allows ATP to hydrolyze without doing work ('slippage'). A detailed account of the ATP used, and of the actual work done, would require simulating random walks on a kinetic diagram representing all state transitions of the macromolecule catalyzing the energy transduction (for instance the Na^+ or Ca^{2+} pump) (Hill, 1989).

al., 2014).

The physiological level of Glu is less sharply delimited in neurons, but assumed to be in the low millimolar range (1–10 mM in Ishikawa et al., 2002). Because the model did not implement the saturating Michaelis-Menten kinetics of enzymatic reactions (Segel, 1984), baseline [Glu] was put to 1 mM, the lower end of the physiological spectrum. From this low baseline concentration, actual reactions involving Glu are more likely to stay in the quasi-linear regime, given, for instance, K_{m} values for the vesicular Glu transporters VGLUT1-2 between 1.9 and 3.4 mM (Herzog et al., 2001).

Substituting the first two conditions ([Glu] = 1 mM and [ATP] = [P_i] = 1.5 mM at $w = 1$) into equations 4 and 5, along with [Gln] = 0.4 mM and [Pyr] = 0.04 mM (Table 1), gives

$$\begin{cases} \kappa_1 = \dfrac{1}{0.6}\,\kappa_2 \\ \kappa_3 = 25\,(1.5\,\kappa_2 + 1). \end{cases} \tag{6}$$

As third constraint was used the approximate 1:1 relationship that has been observed between the rate of glucose (Glc) oxidation, V_{Glc}, and the rate of Glu-Gln cycling, V_{Glu} (Dienel, 2019; Rothman, Behar, & Dienel, 2024; Sibson et al., 1998, but see also Danbolt (2001) and Lieth et al. (2001)). This constraint implies that for each Glc molecule oxidized, the axon bouton exchanges one Glu molecule for one Gln with the astrocyte. Let $\mathrm{ATP}_{\mathrm{Glc}}$ denote the number of ATP molecules produced by the degradation of one molecule of glucose (32 in Dienel (2019); 33.6 in Yu et al. (2018)), and $\mathrm{ATP}_{\mathrm{Glu}}$ the 1.5 ATP molecules the axon hydrolyzes for the recycling of one molecule of Glu (0.5 for vesicle acidification and one for the entry of Gln), then the above 1:1 ratio of V_{Glu} to

V_{Glc} can be achieved only if, using equations 4 and 5,

$$\begin{aligned}\frac{\mathrm{ATP_{Glu}}}{\mathrm{ATP_{Glc}}} = \frac{1.5}{32} = 0.047 &= \frac{1.5\ \kappa_2\ [\mathrm{Glu}]\ [\mathrm{ATP}]^2}{1.5\ \kappa_2\ [\mathrm{Glu}]\ [\mathrm{ATP}]^2 + w[\mathrm{ATP}]^2} \\ &= \frac{1.5\ \kappa_2\ [\mathrm{Glu}]}{1.5\ \kappa_2\ [\mathrm{Glu}] + w} \\ &= \frac{1.5\ \kappa_2}{1.5\ \kappa_2 + 1\ \mathrm{s^{-1}}},\end{aligned} \tag{7}$$

from which, using equation 6,

$$\begin{cases} \kappa_1 = \dfrac{1}{18.3} & \mathrm{mM^{-2}\ s^{-1}} \\ \kappa_2 = \dfrac{1}{30.5} & \mathrm{mM^{-1}\ s^{-1}} \\ \kappa_3 = \dfrac{800}{30.5} & \mathrm{mM^{-2}\ s^{-1}}. \end{cases} \tag{8}$$

With these parameter values, the three negative terms of equation 2 represent 1.6 %, 95.3 % and 3.1 %, respectively, of the baseline ATP consumption.

2.4 Validation of the model

First, the model's rate of vesicular Glu accumulation (second term of equation 1) was compared with that of actual synaptic boutons. Following the numerical data of Attwell and Laughlin (2001) (baseline spike rate of 4 Hz and release probability of 0.25), one vesicle has to be refilled per second. To refill a vesicle of 4,000 molecules in a presynaptic varicosity of volume 0.125 $\mu\mathrm{m}^3$ (Shepherd & Harris, 1998), a mean transport rate per volume is needed of

$$\frac{4000}{0.125\ 10^{-18}} \frac{\mathrm{molecules}}{\mathrm{m^3\ s}} = \frac{664.2\ 10^{-23}}{0.125\ 10^{-18}} \frac{\mathrm{moles}}{\mathrm{m^3\ s}} = 0.0531\ \mathrm{mM\ s^{-1}}.$$

Put another way, if 4,000 Glu molecules are translocated per second from the cytosolic pool to the vesicle pool, then [Glu] falls at a rate of 0.0531 $\mathrm{mM\ s^{-1}}$, which is comparable to the baseline value of the second term of equation 1 (0.0492 mM $\mathrm{s^{-1}}$).

Table 2: Estimated Workload of a Presynaptic Mitochondrion [a]

Work	ATP molecules used	Correction	ATP/synapse/s
Glu recycling	1.5 per Glu molecule [b]	$\times$ 4,000	6,000
Ca^{2+} extrusion	12,000 per vesicle [c]		12,000
Exo-/endocytosis	821 per vesicle [c]		821
Action potentials [d]	$3.90e^8$ per axon [c]	$/8,000$	48,700
Resting potential [d]	$3.40e^8$ per neuron [c]	$/2/8,000$ [e]	21,250
Total signaling			88,771
Housekeeping [d]	1/3 of signaling [c]		29,590
Total			118,361

[a] Data for a neuron firing at 4 Hz and releasing one vesicle of 4,000 Glu molecules at each of its 8,000 release sites per second (Attwell & Laughlin, 2001; Howarth, Gleeson, & Attwell, 2012).

[b] See section 2.2.

[c] Supplementary Spreadsheet of Howarth et al. (2012).

[d] Assuming that presynaptic mitochondria carry the workload of the entire axon, as only 8 % of the axonal mitochondria in Shepherd and Harris (1998) were 'solitary' (not located at synapses).

[e] Assuming that axons and dendritic trees have the same membrane surface area (Lennie, 2003).

Next the model's rate of ATP production was compared with that of a presynaptic mitochondrion. Since the cycling of each of the 4,000 Glu molecules in a vesicle is coupled to the oxidation of one glucose molecule (section 2.3), ATP is produced in the model at a baseline rate of 4,000 $\times$ 32 = 128,000 molecules per second. This rate is comparable to the workload assessed for a presynaptic mitochondrion in Table 2 (118,361 ATP molecules per second), and to the rate of ATP production in computational models of reconstructed presynaptic mitochondria (Garcia et al., 2019, 2023).[4]

In summary, these comparisons justify the choice of w = 1 s^{-1} as baseline workload in section 2.3.

2.5 Model variants

Table 3: Model and Variants Based on Equations 1 and 2

	model	variant I	variant II
Parameters \ constants	$\omega \propto w$	ω = 1	[Glu] = 1 mM
Control by ATP potential	+	+	+
Expansible Krebs cycle	+	+	–
w-Dependent Glu formation	+	–	–

Table 3 summarizes the characteristics of the model and of two incomplete variants. The default model of equations 1 and 2 takes for ω the value of Table 1. Variant I is

[4] This workload is greater, however, than that estimated by Garcia et al. (2019, their supplementary section S2.1), as these authors counted only the ATP needed for Glu packaging and vesicle release (first three rows of Table 2).

identical to this full model but for the value of ω, which is clamped at unity for all workloads w. In other words, Glu is formed by the PAG enzyme at a rate $\kappa_1[\mathrm{Gln}][\mathrm{P_i}]^2$ that is independent of the activity of the synapse. In variant II, the cytosolic Glu concentration remains constant at 1 mM, making equation 1 superfluous. Only equation 2 is solved, but with its last term ('Gln import') replaced by κ_2 $[\mathrm{Glu}]$ $[\mathrm{ATP}]$, as only so much Gln is imported as is needed to replace the Glu accumulated into vesicles.

2.6 Numerical methods and code availability

The models were implemented in XPPAUT (Ermentrout, 2002) and numerically integrated with backward-Euler or second-order Runge-Kutta, using a fixed step size of 10 ms (100 ms for the figures). The XPP scripts will be made available at ModelDB (https://modeldb.science).

3 Analytical and numerical results

Sections 3.1–3.4 analyze the [ATP] and [Glu] responses to varying workloads. The full model's ability to reproduce experimental data from the literature is demonstrated in section 3.5.

3.1 Steady-state responses

Figures 2A–C plot the nullclines of the three models of Table 3 for a variety of workloads. In the full model (Figure 2A), the nullcline of equation 1 varies with w in such a manner that it always intersects its counterpart of equation 2 at an ATP level of 1.5

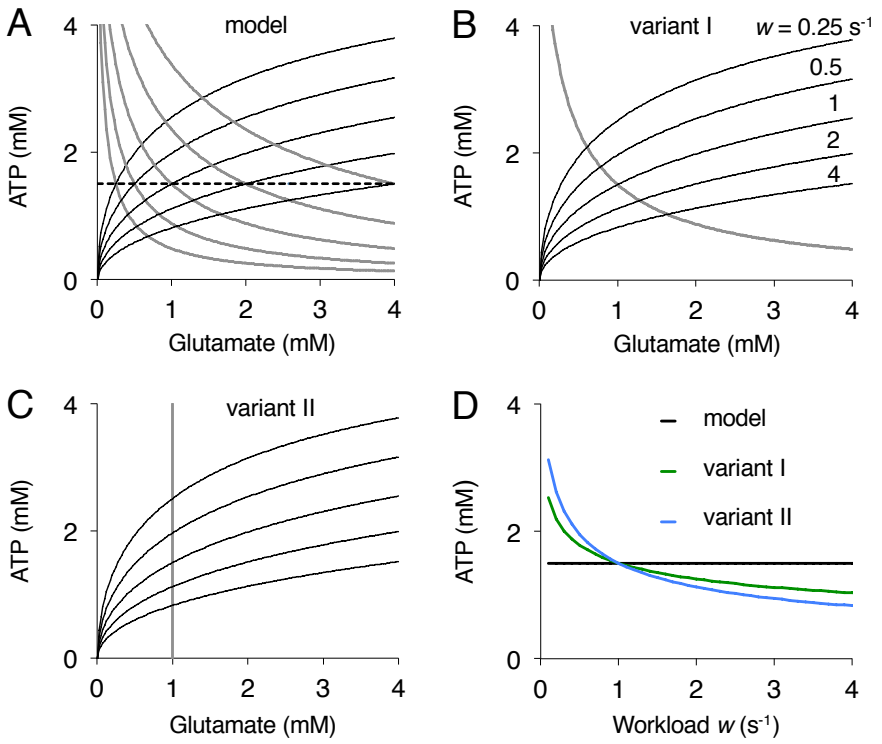

Figure 2: Steady-state responses to varying workloads in the full model and its variants I and II of Table 3. (A-C) Nullclines of equations 1 (gray curves) and 2 (black) for the five workloads indicated in panel B. (D) Steady-state ATP concentration as a function of w in the full model (black), variant I (green) and variant II (blue).

mM (see horizontal line). In contrast, in model variant I, the nullclines of equation 1 for varying values of w coincide (Figure 2B), whereas the dynamics of variant II is limited to motion on the line [Glu] = 1 mM (Figure 2C). The error-free steady-state ATP level in the full model (black curve in Figure 2D) contrasts with the decline of [ATP] with w in variants I and II (green and blue), demonstrating the importance of workload-dependent variations in the rate of Glu formation and in the size of the Krebs cycle (Table 3).

The invariance of the steady-state ATP level to w, and some other characteristics of

the full model, are easily proven in the following theorems and corollaries.

Theorem 1. *If ω is taken proportional to w in equations 1 and 2, then the steady-state concentration of ATP is independent of the workload w.*

Proof. Solving equation 5 for [Glu] gives

$$[\mathrm{Glu}] = \frac{w\,[\mathrm{ATP}]^2}{\kappa_3\,[\mathrm{Pyr}]\,[\mathrm{P_i}]^2 - 1.5\,\kappa_2\,[\mathrm{ATP}]^2}, \tag{9}$$

which, after substitution into equation 4, yields

$$\omega\,\kappa_1\,[\mathrm{Gln}]\,[\mathrm{P_i}]^2 = \kappa_2\,[\mathrm{ATP}]\frac{w\,[\mathrm{ATP}]^2}{\kappa_3\,[\mathrm{Pyr}]\,[\mathrm{P_i}]^2 - 1.5\,\kappa_2\,[\mathrm{ATP}]^2}.$$

Dividing throughout by $w \neq 0$ reveals that [ATP] does not depend on the workload, and hence must assume its baseline value of 1.5 mM. □

Theorem 1 holds irrespective of the values of parameters κ_{1-3} and of the relationship between $[\mathrm{P_i}]$ and [ATP] (equation 3). The invariance of steady-state [ATP] to w requires, however, 1) that the rate of Glu formation varies in proportion to the workload w, 2) that the rate of ATP production depends on [Glu] (hence that the Krebs cycle can expand), and 3) that the rate of vesicular Glu accumulation depends on [ATP].

Theorem 2. *If ω is taken proportional to w in equations 1 and 2, then the steady-state concentration of Glu is proportional to the workload w.*

Proof. From [ATP] = [P_i] = 1.5 mM at steady state for all workloads w (theorem 1), equation 9 reads, for a workload $w = C\ \mathrm{s}^{-1}$,

$$\begin{aligned}[\mathrm{Glu}] &= \frac{C\ \mathrm{s}^{-1}}{\kappa_3\,[\mathrm{Pyr}] - 1.5\,\kappa_2} \\ &= C\ \mathrm{mM}.\end{aligned}$$

Hence, at steady state, [Glu] is a sensor of the workload w. □

A sublinear increase of [Glu] is obtained by replacing in equations 1 and 2 all linear dependencies on [Glu] by dependencies on [Glu]^n, in which case the invariance of [ATP] to w still holds, but with [Glu] being proportional to $\sqrt[n]{w}$.

A limitation of the model must also be mentioned here. Because [Gln] is taken constant in the first term of equation 1 (see section 2.2.2), the model is unable to reproduce the observed depletion of Glu after high-frequency stimulation, which has been attributed to a failing supply of Gln by astrocytes (Tani et al., 2014).

Corollary 1. *At steady state, the rates of ATP production, Glu formation and vesicular Glu accumulation are proportional to the workload w.*

Proof. For $w = C\ \mathrm{s}^{-1}$, this corollary directly follows from substituting C mM for [Glu] in the corresponding terms of equations 1 and 2. □

By the following argument, corollary 1 can be extended, with some caution, to the (non-modeled) rate of vesicle *release*. In equation 1, the rate at which Glu is sequestered by the virtual pool of vesicles does not saturate. In actual axon boutons, however, the pool of vesicles and the number of Glu molecules per vesicle are limited to a few hundred and thousand, respectively (Dittman & Ryan, 2009; Wang et al., 2019). Hence the model's unlimited apparent storage capacity is biologically only feasible if the vesicle pool is not only filled, but also emptied, at a rate proportional to the workload.

Corollary 2. *At steady state, the fraction of ATP the axon spends on Glu release and recycling is independent of the workload w.*

Proof. For $w = C$ s^{-1}, this corollary follows directly from substituting C mM for [Glu] in equation 7. □

This corollary implies that the presumed 1:1 coupling between the rates of glucose consumption and Glu-Gln cycling (section 2.3) holds at all values of w. Such an invariance has important consequences for the interpretation of labeling and imaging experiments, as it justifies averaging these rates within a voxel of neurons with potentially disparate workload (Mason et al., 1995; Sibson et al., 1998).

3.2 Dynamical responses to time-varying workloads

Figure 3 plots the responses of the full model and its two incomplete variants (see Table 3) to a rectangular increase (left panels) or decrease in workload (right). The sequence of events is first described for the full model (black traces).

A sudden increase in workload causes a fall in [ATP] (panel A), attended by a rise in [Glu] (panel B) as less ATP is available to accumulate Glu into vesicles. The rate of ATP production (panel C) climbs in two phases: a fast and a slow phase. The steep rise coincides with the fall in [ATP] and reflects the quasi-static control by the (reduced) ATP potential[5] (see equation 2). This fast phase can be attributed to the allosteric

[5] This steep rise (50 % in 1 s) may be too fast to be generated by the oxidation of glucose, but actual neurons can rapidly liberate a limited amount of ATP in the creatine phosphokinase reaction (Erecińska & Silver, 1989; Sauter & Rudin, 1993). The steep rise can be smoothed, without changing the peak rate of ATP production, by using simpler expressions for the (inverse) phosphorylation potential, such as [P_i][ADP] or [P_i].

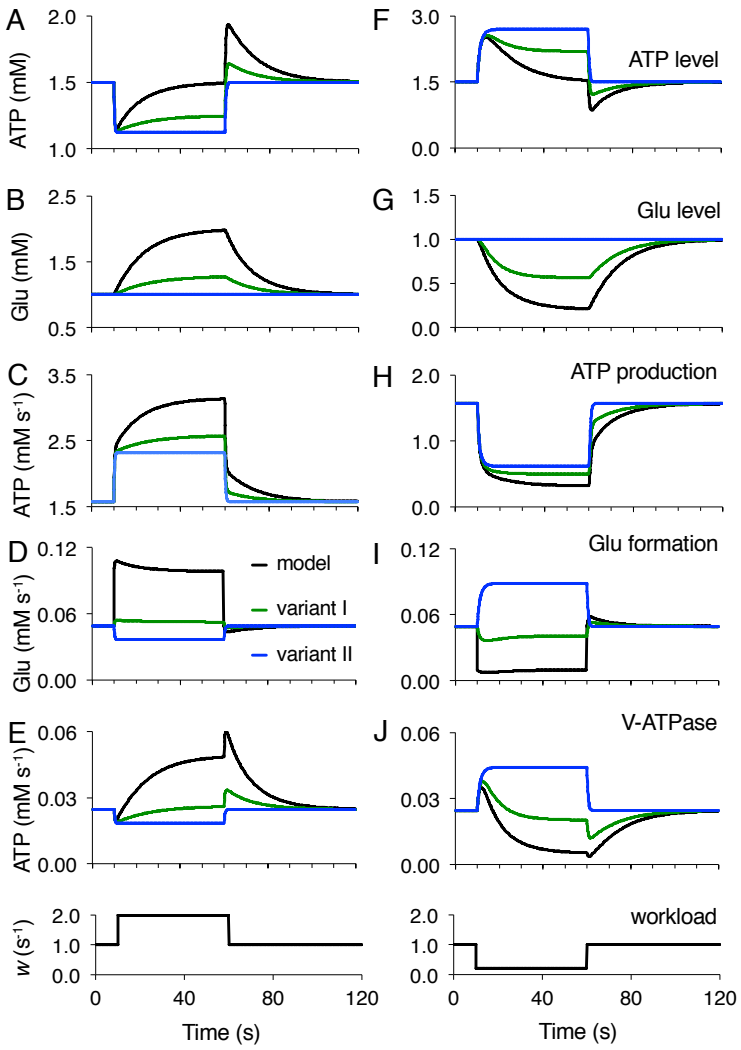

Figure 3: Responses of the full model and its variants I and II of Table 3 to a rectangular increase by 100 % (panels A–E) or decrease by 80 % (F–J) in workload (see stimulus in bottom traces). The panels plot the cytosolic concentration of ATP (A and F) and Glu (B and G); the rate of ATP production (C and H, first term of equation 2); the rate of Glu formation (D and I, first term of equation 1); and the rate at which ATP is hydrolyzed by vesicular V-ATPase activity (E and J, second term of equation 2).

actions of ATP ($-$) and ADP ($+$) on the enzymes involved in ATP production (see section 2.2.3), and its effect is to reduce the amplitude of the [ATP] transients (not shown). The slow phase of enhanced ATP production, in contrast, closely follows the rise in [Glu]. It reflects the expansion of the Krebs cycle, and restores ATP to its baseline level (see panel A).

The rate of Glu formation (panel D) increases with the workload (see equation 1), and remains high with only a small adaptation when [ATP] and [P_i] return to baseline. Together, the restoration of [ATP] and the sustained elevation of [Glu] cause more Glu to be accumulated into vesicles (panel E). The decrease in workload at 60 s evokes a rebound peak of the ATP level (panel A), similar in shape to the response transient in (F). Overall, the responses in panels F–J are mirror images of the left-column responses.

In model variant I (green traces in Figure 3), the rate of Glu formation, now depending only on [P_i], cannot keep up with the workload (panel D). The resulting weak rise in [Glu] (panel B) and restricted expansion of the Krebs cycle (panel C) fail to restore ATP to its baseline level (panel A).

In variant II (blue traces in Figure 3), the Glu level is constant (panel B), so that the production of ATP (panel C) can only be stimulated by a persistent error signal (the reduced ATP potential). Like variant I, variant II settles at a sub-baseline level of ATP, at which also the rate of ATP consumption for Glu accumulation is below that in the full model (panel E). An advantage of variant II is the absence of a rebound peak, and one may argue that ATP homeostasis would improve if the gain of the error signal were increased, for instance by raising the ATP potential to a power q (but see footnote 5). Large values of q would be needed, however, to restore ATP to within

$\pm$ 10 % (0.15 mM) of its baseline level ($q > 3.8$ and $q > 9.8$ for the left and right column, respectively).

3.3 The amount of energy spent on Glu-Gln cycling determines the speed of ATP homeostasis

The futile rebound of the ATP level evoked by the return to baseline of an enhanced workload (see black trace in Figure 3A) can be reduced by increasing the percentage of energy that is spent on the vesicular accumulation of Glu. In Figure 4, this percentage was varied by changing parameter κ_2 (the rate-constant of vesicle acidification), after which equation 6 was used to adjust the values of κ_1 and κ_3, so as to keep ATP and Glu at their baseline levels of Table 1. The fraction of energy spent on Glu cycling was then calculated from equation 7. Dividing and multiplying κ_2 by a factor of four changed the fraction of energy spent on Glu cycling from its default value of 4.7 % to 1.2 % and 16.4 %, respectively (see legend to Figure 4A).

The time-constant of ATP homeostasis, as assessed from the time needed for [ATP] to fall by 63.2 % to baseline from the rebound peak in Figure 4A, scaled in inverse proportion to the energy spent on Glu cycling, decreasing from 55.4 s (model with 1.2 % energy spent on cycling) to 14.2 s (4.7 %) and 3.8 s (16.4 %). Note that the narrowing of the rebound peak in the 'fast' model (red curve) is the result of a faster vesicular Glu accumulation (larger κ_2), whereas the narrowing of the negative transient after stimulus onset must be attributed to the larger values which κ_1 and κ_3 had acquired after recalibration of the model (see caption to Figure 4).

Although the duration of futile ATP production could thus be reduced by spending

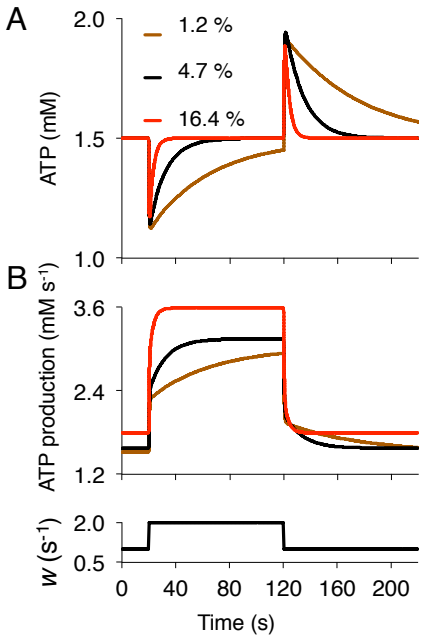

Figure 4: The percentage of energy spent on Glu-Gln cycling determines the speed of ATP homeostasis. (A) Cytosolic ATP concentration. (B) Rate of ATP production. The workload w of the (full) model was doubled during a 100-s interval (bottom panel). The three illustrated models varied by the percentage of the ATP they spent on Glu cycling: 1.2 % (brown curve), 4.7 % (default model, black) and 16.4 % (red). These percentages were produced by varying parameter κ_2, followed by a recalibration of the model as explained in section 3.3. The resulting parameter values were, in order of ascending energy fraction: κ_1 0.0136, 0.0546 and 0.219 $\mathrm{mM}^{-2}\ \mathrm{s}^{-1}$; κ_2 0.0082, 0.0328 and 0.131 $\mathrm{mM}^{-1}\ \mathrm{s}^{-1}$; κ_3 25.3, 26.2 and 29.9 $\mathrm{mM}^{-2}\ \mathrm{s}^{-1}$.

more energy on Glu-Gln cycling, this strategy also enhanced the baseline rate of ATP production (from 1.52 to 1.57 and 1.8 mM s^{-1} in Figure 4B). Nevertheless, in the brown trace of Figure 4A, the ATP in the rebound peak would have sufficed to raise during 410.6 s the baseline rate of ATP production from 1.52 mM s^{-1} to the default value of 1.57 mM s^{-1}, in the mean time ensuring a more precise ATP homeostasis. It must therefore be concluded that the optimal amount of energy a neuron should spend on Glu-Gln cycling depends on the statistics of its workload (the interval between transitions, and their shape).

3.4 Quality and cost of ATP homeostasis

To take into account the effect of the response transients, the quality of ATP homeostasis was also assessed from the statistics of the ATP concentration sampled during a rectangular modulation of the workload w with period T

$$w(t) = 2 + 1.5 \, \mathrm{sign}(\sin \frac{2\pi}{T} t). \tag{10}$$

Figure 5A measures the accuracy of homeostasis as the mean absolute deviation of [ATP] from the target value of 1.5 mM. The ATP level deviated considerably from the target value in model variants I and II (green and blue curves). Only at the smallest periods T did these variants outperform the full model (black), in which the transients then dominated the response. The deviation was smallest, as expected, in the model of Figure 4 spending 16.4 % of its energy on Glu-Gln cycling (red).

These findings are confirmed in Figure 5B, which plots the correlation between the [ATP] trace (minus its target value of 1.5 mM) and the workload $w(t)$ (minus its average value of 2 s^{-1}). Negative values indicate either work which ATP failed to do because its

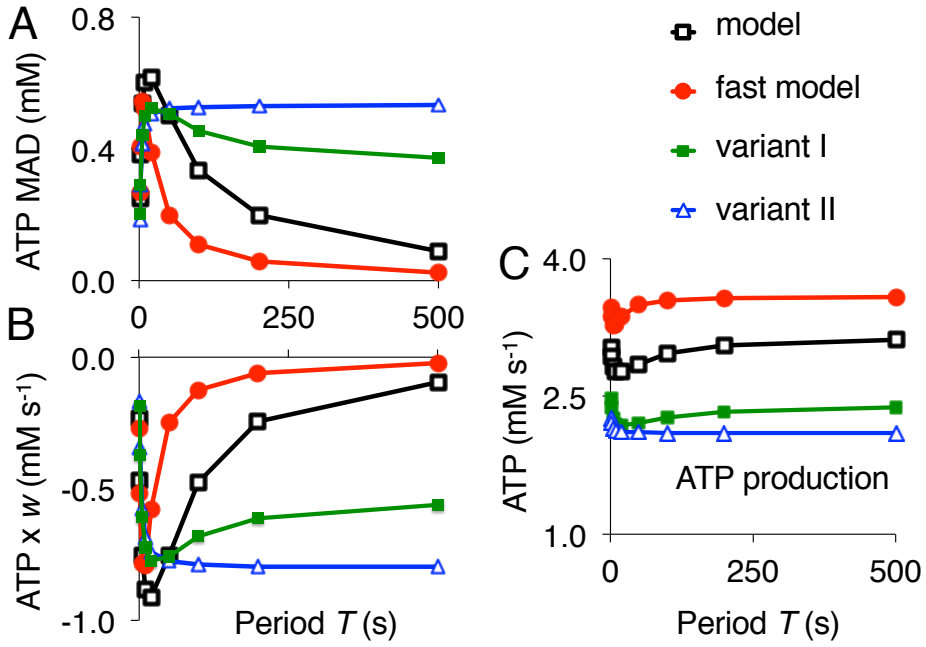

Figure 5: Quality (A and B) and cost (C) of ATP homeostasis in the full model and its variants I and II of Table 3 (same color code as in Figure 3). The red curve, labelled 'fast model', was produced by the model spending 16.4 % of its energy on Glu cycling (see Figure 4). (A) Mean absolute deviation (MAD) of [ATP] from the target level of 1.5 mM. (B) Correlation between [ATP] and workload w. (C) Mean rate of ATP production. For a detailed description see section 3.4.

concentration was less than 1.5 mM (for instance during the initial dip in Figure 3A), or futile work done when [ATP] exceeded 1.5 mM (such as during the rebound peak).

Figure 5C demonstrates that only the full model (black) and its 'fast' version (red) were able to double their mean rate of ATP production in response to the doubling of the average workload in equation 10. Although in both models the error function approached zero when the period T increased (panels A and B), the cost of homeostasis in terms of ATP production was larger in the 'fast' model. Hence at low frequencies of workload variation (high T), the benefit of spending extra energy on ATP homeostasis is small.

3.5 Reproduction and reinterpretation of experimental data

In Figure 6, each parameter κ_{1-3} was varied separately (without recalibrating the model). The obtained effects were consistent with published observations, as argued below.

Reducing κ_1 (the rate-constant of Glu formation) diminished [Glu] (gray trace in Figure 6A), thereby replicating experiments in which either the Gln synthase (Tani et al., 2014) or the P_i-activated glutaminase were inhibited (see Hertz, 2004; Marx et al., 2015), or in which the astrocytic connexin 43 was knocked out (Cheung et al., 2023). The ATP level declined in concert with [Glu] (black trace).

The model predicts different outcomes for experiments that selectively manipulated either the second term ('vesicle acidification') or the third term ('work') of equation 2. From theorem 1, a decrease in workload should have no effect on the steady-state level of ATP, whereas impairing Glu disposal (reducing κ_2) is predicted to raise [ATP] (Figure 6B). In agreement herewith, Rangaraju et al. (2014, their Figure 2A) observed that

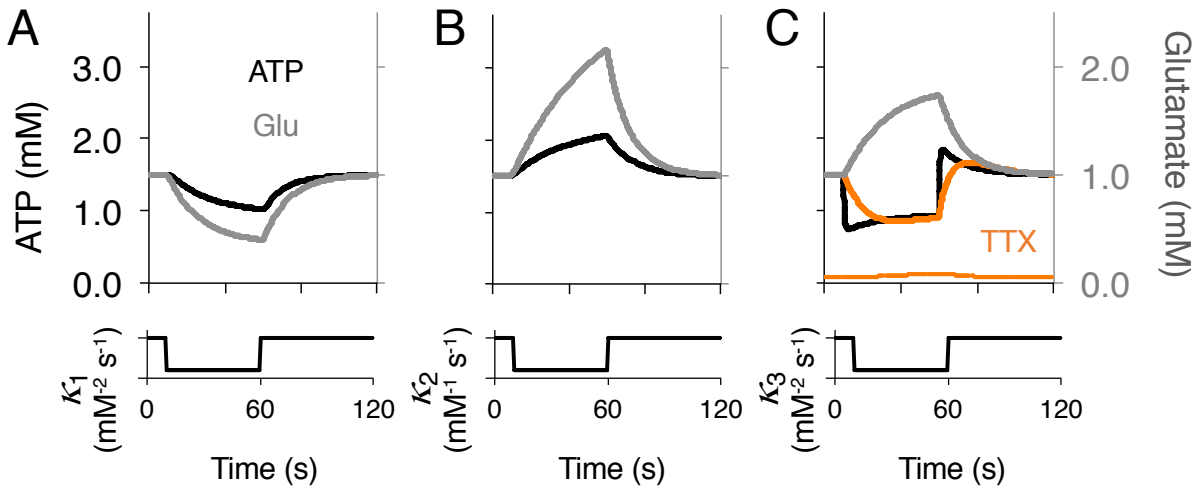

Figure 6: Time-course of the cytosolic concentrations of ATP (black traces, left vertical axis) and Glu (gray, right axis) during a 50-s rectangular reduction by 80 % of the parameter in the corresponding bottom panel (see Table 1 for the default parameter values). These parameters specify the rate of Glu formation (κ_1, panel A), the rate of vesicular Glu accumulation (κ_2, B), and the rate of ATP production (κ_3, C). All simulations started from the default concentrations [ATP] = 1.5 mM and [Glu] = 1 mM, with workload w = 1 s^{-1}, except in panel C, where the orange curves, simulating preincubation with tetrodotoxin, were obtained with w = 0.05 s^{-1}, and hence with a baseline [Glu] of 0.05 mM.

the ATP level was not different in axon terminals chronically incubated in tetrodotoxin (TTX, a blocker of voltage-gated Na^+ channels), consistent with the invariance of [ATP] to w. In contrast, [ATP] rose to > 2 mM when exocytosis was eliminated (Figure 2A of Rangaraju et al., 2014), a rise reproduced by the black trace in Figure 6B. In a continuation of these experiments, Pulido and Ryan (2021, their Figure 1) observed that blocking the Na^+ pump with ouabain did not, whereas blocking the vesicular V-ATPase did, raise [ATP], again in agreement with the predictions of the model. It is not straightforward, however, to deduce from the rise in [ATP] the amount of energy consumed by the silenced process. In Figure 6B, for instance, [ATP] rose towards a new steady state of 2.25 mM, an increase by 50 %, even though the inhibited process, vesicle acidification, consumed at baseline only 1.6 % of the ATP production (section 2.3).

In an additional experiment, Rangaraju et al. (2014, their Figure 2C) found that when the ATP production was blocked, the ensuing decline of [ATP] was slower in slices incubated in TTX. This experiment can be simulated by reducing κ_3 (the rate-constant of ATP production) either upon the default workload of 1 s^{-1}, or upon a reduced w of 0.05 s^{-1}, the latter mimicking the TTX condition. The slower decline of [ATP] in the presence of TTX (orange curve in Figure 6C) is then readily understood from an inspection of equation 2: as w is the rate-constant of the work term, reducing its value naturally increases the response time-constant.

4 Discussion

An analytical model of the production and consumption of ATP in a presynaptic axon bouton supports the hypothesis that the cycling of glutamate and glutamine between axon and astrocyte acts as a control circuit for ATP homeostasis. The model required, however, that the formation of Glu increased with the workload, from which an increased release then followed by virtue of corollary 1 (see section 3.1). Section 4.1 describes biological processes underlying such an activity-dependent Glu formation. The model's predictions that the capacity of the Krebs cycle, and the cytosolic Glu level, should vary with the workload are discussed in sections 4.2 and 4.3.

4.1 Biophysical mechanisms of activity-dependent glutamate formation

The proportionality between ω and w (between the rate of Glu formation and the workload) is an essential feature of the model: in its absence ATP homeostasis was poor (see model variant I of Table 3, represented by the green curves in Figures 2D, 3 and 5). The imposed proportionality reflects the expected correlations between a variety of biological processes: on the one hand between the rate of Glu release (evoked as it is by action potentials and voltage-gated Ca^{2+} channels) and the workload; on the other hand between the rate of Glu release and the formation and release of Gln by astrocytes. Put another way, the covariation of ω with w closes the Glu-Gln cycle.

In addition to this re-entry mechanism, feedforward interpretations are feasible in which the axon bouton anticipates an increased need for glutamate. For instance, Che-

ung et al. (2022) found that a local rise in the extracellular concentrations of K^+ and Glu, elicited by synaptic activity, opened connexin 43 hemichannels through which the astrocyte released Gln into the perisynaptic space. In this manner Gln (and other small molecules such as citrate, serine and lactate) can be funneled from a large reservoir of gap-junction-coupled astrocytes toward active synapses. Furthermore, the same signal, extracellular K^+, enhanced the conductance of gap junctions and activated the *de novo* synthesis of Gln (see Dienel, 2019, p. 968). Other feedforward mechanisms justifying ω to covary with w are the activity-induced expression of a presynaptic Gln transporter (Erickson, Kyllo, & Wulff, 2023), and the observation that vesicular Glu transporters act as Na^+-driven phosphate carriers when they are exposed to the extracellular fluid during exocytosis (Bellocchio et al., 1998). The P_i accumulated in the presynaptic bouton by these transporters (Cheret, Ganzella, Preobraschenski, Jahn, & Ahnert-Hilger, 2021) can activate the PAG enzyme and stimulate Glu formation (see appendix section B.1).

4.2 Variation of the size of the pool of Krebs cycle intermediates

In the model, part of the newly formed Glu was inserted as αKG in the Krebs cycle. The pool of Krebs cycle intermediates shrank, in turn, through the release of Glu as neurotransmitter. At steady state, both processes were balanced. Although the use of (cytosolic) [Glu] as a surrogate for the mitochondrial concentration of αKG may suggest that the Krebs cycle is expanded solely by Gln and Glu, this need not be the case. Another substance that can fill the Krebs cycle is citrate. Like Gln, citrate is profusely released by astrocytes, and reaches an equally high concentration of 0.4 mM in the cerebrospinal fluid (Westergaard et al., 2017). Citrate is driven into neurons

by the Na^+-dependent SLC13A5 carrier (Rae et al., 2024), and can be imported into mitochondria through reverse operation of the SLC25A1 carrier (Jiang et al., 2016).

Neurotransmitters less closely connected to the Krebs cycle than Glu may modulate alternative pathways for ATP production, as proposed in appendix C.

4.3 Variation of the cytosolic concentration of glutamate

An increase in workload invariably raised the model's cytosolic Glu concentration (see theorem 2 in section 3.1). Probes for a quantitative measurement of [Glu] are lacking (Wang et al., 2019), but consistent with the prediction of a varying Glu concentration, Hertz et al. (1999, p. 424) concluded that 'brain activation appears to lead to an expansion of the transmitter pool, with its size reverting to normal levels within 15 minutes'. The authors attributed this expansion of the transmitter pool to a temporary dissociation between the *de novo* synthesis of Gln by astrocytes and the eventual oxidation of excess Glu, also by astrocytes (see appendix Figure A1, panels B and C, respectively).

Elevated levels of Glu (by 19 %) and Gln (83 %), but no other metabolites, were observed during epileptic activity (Mangia, Giove, & Dinuzzo, 2012; Peca et al., 2010), and elevated combined Glu-Gln signals were measured after a high-demand cognitive task (Wiehler, Branzoli, Adanyeguh, Mochel, & Pessiglione, 2022). In rats under pentobarbital anaesthesia, the cerebral Glu content decreased by 28 % (Sibson et al., 1998, Table 1). These observed variations are smaller than those generated in the model, but, as noted in the discussion of theorem 2, equivalent models can be constructed in which [Glu] rises sublinearly with w (see section 3.1).

Finally, Magi et al. (2013) observed that ATP production was enhanced in neuronal

cell lines exposed to 0.5–1 mM solutions of glutamate, but only in the presence of Ca^{2+} ions. Clearly, such a Ca^{2+} dependency of ATP production would also reduce the required scale of expansion of the Krebs cycle. The role of Ca^{2+} ions in ATP homeostasis is further discussed in appendix D.

4.4 Conclusion

In a metabolic model of a presynaptic axon bouton, the rate of ATP production increased in proportion to the workload to restore, without error, the physiological ATP level at steady state. Crucial for this precision were workload-dependent variations in the rate of neurotransmitter formation and release. Since, apart from solute transport, no receptor-mediated effects were modeled, ATP homeostasis may be an evolutionarily early function of transmitter release. The model predicts that impaired synthesis or release of neurotransmitter leads to deficient or inappropriate ATP production, a condition thought to underlie neurodegenerative disorders.

Appendix A Presumed circuit of Glu-Gln cycling between axon terminal and astrocyte

Figure A1 depicts the local cycling of Glu and Gln between a presynaptic axon terminal (right) and a perisynaptic astrocyte (left), and the interactions between the flows of Glu and Gln and the fluxes of the respective Krebs cycles (Hertz, 2004). Only the energy budget of the axon was reckoned with in the model (numbers in red). The oxidation of one glucose molecule generates 32 ATP molecules in the axon terminal (Dienel,

2019). In astrocytes, in contrast, the Krebs cycle may be poorly expressed or truncated (Dobolyi et al., 2024); in the figure it serves only for the *de novo* synthesis of Gln from glucose (panel B), and the eventual degradation of Glu (panel C), during increased and decreased workloads of the axon, respectively. Panel A shows a lossless Glu-Gln cycling at steady state.

Figure A1: Presumed circuit of glutamate-glutamine cycling between a presynaptic axon bouton (right) and a perisynaptic astrocyte (left). Red and blue numbers denote energy budgets (in units of ATP molecules) for axon and astrocyte, respectively. (A) Ideal, lossless Glu-Gln cycling between axon and astrocyte at steady state. (B) *De novo* synthesis of Gln in the astrocyte, and expansion of the pool of Krebs cycle intermediates in the axon, upon an increase in (axonal) workload. (C) Degradation of Glu in the astrocyte, and gradual contraction of the pool of Krebs cycle intermediates in the axon, upon restoration of the axonal workload to its baseline level. The labeled pathways are: ① Accumulation of Glu in synaptic vesicles (requiring 0.5 molecules of ATP for each Glu) and release of Glu in the synaptic cleft, on the part of the axon; and the uptake of Glu via a Na^+-driven Glu transporter on the part of the astrocyte. ② Conversion of Glu to Gln by Gln synthase. ③ Release of Gln from the astrocyte, for instance through connexin 43 hemichannels (Cheung et al., 2022), followed by its import into the axon via a Na^+-driven Gln transporter (requiring one ATP molecule to restore the Na^+ gradient). ④ Conversion of Gln to Glu by neuronal phosphate-activated glutaminase. ⑤ Carboxylation of the 3-carbon Pyr to the 4-carbon OAA by astrocytic pyruvate carboxylase. ⑥ Reversible interconversion between the 5-carbons Glu and αKG by a mitochondrial transaminase or Glu dehydrogenase. ⑦ Decarboxylation of the 4-carbon Mal to Pyr by malate dehydrogenase. Abbreviations: acCoA, acetyl-coenzyme A; αKG, α-ketoglutarate; Cit, citrate; Fum, fumarate; Glc, glucose; Gln, glutamine; Glu, glutamate; Mal, malate; OAA, oxaloacetate; Pyr, pyruvate; Suc, succinate. Diagrams partly based on Hertz (2004, Figure 1).

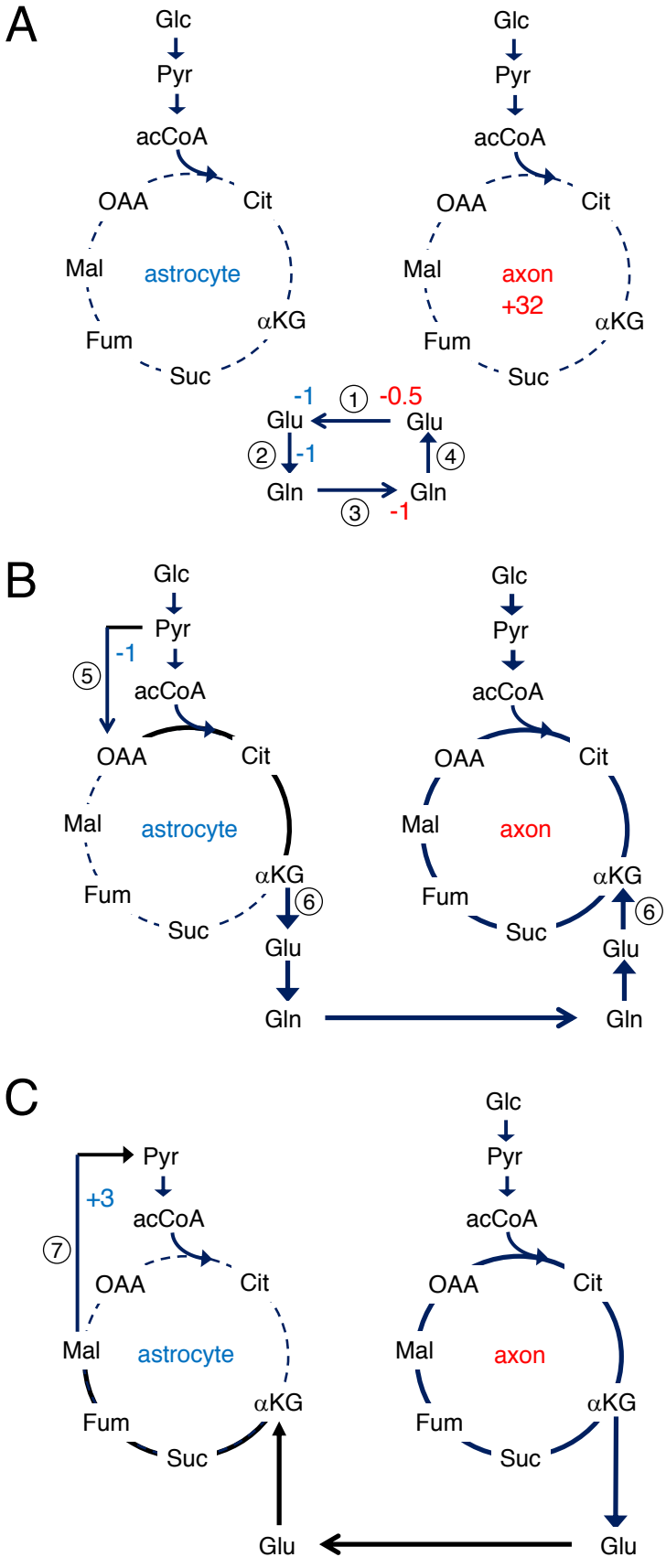
A
Glc
Pyr
acCoA
OAA
Cit
Mal
astrocyte
αKG
Fum
Suc
Glc
Pyr
acCoA
OAA
Cit
Mal
axon
+32
αKG
Fum
Suc
-1
①
-0.5
Glu
Glu
②
-1
④
Gln
Gln
③
-1
B
Glc
Pyr
-1
⑤
acCoA
OAA
Cit
Mal
astrocyte
αKG
Fum
Suc
⑥
Glu
Gln
Glc
Pyr
acCoA
OAA
Cit
Mal
axon
αKG
Fum
Suc
⑥
Glu
Gln
C
Pyr
+3
⑦
acCoA
OAA
Cit
Mal
astrocyte
αKG
Fum
Suc
Glu
Glc
Pyr
acCoA
OAA
Cit
Mal
axon
αKG
Fum
Suc
Glu

Appendix B Constituent reactions of the model

This appendix describes in greater detail the four reactions introduced in section 2.1, and the assumptions underlying their conversion to equations 1 and 2. Where available, alternative reactions are also given.

B.1 Formation of glutamate by phosphate-activated glutaminase

Glutamine supplied by the astrocyte is hydrolyzed in the axon bouton to Glu and ammonia to replenish the Glu stored in synaptic vesicles:

$$\text{L-Glutamine} + \text{H}_2\text{O} + 2\text{P}_\text{i} \rightarrow \text{L-glutamate} + \text{NH}_3 + 2\text{P}_\text{i}. \tag{B1}$$

The ammonia equilibrates rapidly (within 100 ms) (Cooper & Plum, 1987), and is almost completely used by astrocytes for the reamidation of Glu to Gln (Cooper & Jeitner, 2016). The reaction is therefore *de facto* irreversible.

The dimeric phosphate-activated glutaminase (PAG) has a linear rate dependency on the concentration of the precursor Gln, and a parabolic dependency on that of the positive allosteric modulator P_i, which counteracts the inhibitory action by the reaction product Glu (Tveit et al., 1970). According to Erecińska and Silver (1990, p. 262), however, Glu plays little role in modulating PAG activity in neurons, as opposed to astrocytes. Kvamme et al. (2001) suggested that the enzyme is located on the outer surface of the inner mitochondrial membrane (Figure 1), but it is still unclear whether its active sites face the cytosol or the matrix (Rae et al., 2024). Given a K_a value of 6 mM for the P_i-activation of PAG (Hogstad et al., 1988), the cytosolic [P_i] was used, which is an order of magnitude lower than that of the matrix (Stern et al., 2023).

The Na^+-driven entry of Gln into the axon terminal (Varoqui et al., 2000), and the preferential uptake of Gln by synaptic mitochondria (Erecińska & Silver, 1990, p. 250), were assumed not to be rate-limiting for Glu formation, and these reactions were therefore not modeled. The extra ATP needed to restore the Na^+ gradient, however, is accounted for by the last term of equation 2.

B.2 Interconversion between glutamate and α-ketoglutarate

The transamination reaction catalyzed by the mitochondrial enzyme glutamate-pyruvate aminotransferase GPT2 (EC 2.6.1.2, or alanine transaminase) is used for the interconversion of Glu and the Krebs cycle intermediate αKG:

$$\mathrm{Pyruvate_m} + \text{L-glutamate}_\mathrm{m} \rightleftharpoons \text{L-alanine}_\mathrm{m} + \alpha\text{-ketoglutarate}_\mathrm{m}. \tag{B2}$$

The enzyme has been detected in both the cytosolic and mitochondrial fractions of synaptosomes (Erecińska, Nelson, & Silver, 1996, p. 22), but neurons preferentially express the mitochondrial isoform GPT2: their GPT2/GPT1 ratio is six times that in astrocytes (Baytas, Davidson, DeBerardinis, & Morrow, 2022). The essential role of GPT2 in replenishing the Krebs cycle is supported by the depletion of several intermediates in GPT2-null mice (Baytas et al., 2022; Ouyang et al., 2016).

As for the 3-carbon substrates of the GPT enzyme, $[\mathrm{Pyr}]_\mathrm{m}$ was taken constant to satisfy the required mass balance between glycolysis and Krebs cycle (section 2.2.3). L-alanine (Ala), on the other hand, has been proposed to be shuttled from neurons to astrocytes, to be reconverted there to pyruvate by the cytosolic GPT1 (Cooper & Jeitner, 2016; Das, Gauthier-Coles, Bröer, & Rae, 2022). Since the mitochondrial concentration of Ala is three to four orders of magnitude greater than that of αKG (Stern et al., 2023,

Figure 3D and Table S8), relative changes in $[\mathrm{Ala}]_\mathrm{m}$ will be negligible compared to those of $[\alpha\mathrm{KG}]_\mathrm{m}$, and $[\mathrm{Ala}]_\mathrm{m}$ was therefore taken constant at an undetermined value. With both $[\mathrm{Pyr}]_\mathrm{m}$ and $[\mathrm{Ala}]_\mathrm{m}$ constant, $[\alpha\mathrm{KG}]_\mathrm{m}$ is proportional to $[\mathrm{Glu}]_\mathrm{m}$ at steady state (see further appendix section B.3).

Two other mitochondrial enzymes convert Glu to αKG in neurons: glutamate dehydrogenease (GDH) and aspartate aminotransferase (AAT). The reaction catalyzed by GDH depends on the NAD redox potential (using both NAD^+ and NADP^+ as coenzyme) (Cooper & Jeitner, 2016; Nelson & Cox, 2013):

$$\text{L-Glutamate}_\mathrm{m} + \mathrm{NAD(P)}^+ + \mathrm{H_2O} \rightleftharpoons \alpha\text{-ketoglutarate}_\mathrm{m} + \mathrm{NH_4^+} + \mathrm{NAD(P)H}. \quad \text{(B3)}$$

Thermodynamically the reaction favors the formation of Glu (Engel & Dalziel, 1967), but the rapid removal of ammonia (see appendix section B.1) poises it towards the formation of αKG (Cooper & Jeitner, 2016). Strong GDH activity was detected in synaptosomes (Erecińska & Silver, 1990, p. 258), and the synaptosomes from GDH-deficient mice were not able to enhance their respiration when the energy demand increased (Hohnholt et al., 2018). Under the present, simplifying modeling conditions (constant concentrations of Pyr and Ala, ammonia being rapidly removed, and the NAD redox potential rapidly readjusted), the GPT2 and GDH reactions would be indistinguishable.

The strong activity of AAT in synaptosomes (Erecińska & Silver, 1990) would, in addition to converting Glu to αKG, withdraw oxaloacetate from the Krebs cycle, thus annihilating the anaplerotic effect of Glu. The reversible AAT reaction is thought to maintain the balance between the pools of different Krebs cycle intermediates (Erecińska et al., 1996, p. 22). As αKG was taken the sole representative of the Krebs cycle, this

reaction was not modeled [6].

B.3 Bidirectional glutamate transport via the mitochondrial glutamic acid carrier

Most enzymes catalyzing reactions of Glu are located in the mitochondria (Danbolt, 2001). Bidirectional transport of Glu across the inner mitochondrial membrane is implemented by proton-glutamate symporter carriers (GC1 and GC2, see Das et al., 2022):

$$\text{L-Glutamate}_\text{c} + \text{H}^+_\text{c} \rightleftharpoons \text{L-glutamate}_\text{m} + \text{H}^+_\text{m}. \tag{B4}$$

The transport is electroneutral, but as the Glu concentration is higher in the mitochondrial matrix (Stern et al., 2023), a H^+ gradient is needed for Glu to enter (Fiermonte et al., 2002). If this proton gradient is taken constant (Cortassa et al., 2003; Magnus & Keizer, 1997), then the approximation $[\alpha\text{KG}]_\text{m} \propto [\text{Glu}]_\text{m}$ of appendix section B.2 can be extended to $[\alpha\text{KG}]_\text{m} \propto [\text{Glu}]_\text{c}$, the constant of proportionality being absorbed in parameter κ_3.

Although the import of glutamic acid may cause Glu and K^+ to accumulate (Nicholls & Ferguson, 2002), the resulting increase in matrix volume is thought to stimulate ATP production (Juhaszova et al., 2021; Nicholls, Grav, & Lindberg, 1972).

[6] Detailed models of intermediary metabolism (see Rothman et al., 2024) implement the presumed 1:1 ratio of the rate of Gln-Glu cycling to the rate of glucose consumption by coupling the Gln-Glu cycle to the malate-aspartate shuttle, of which the AAT is an essential component (Borst, 2020). In the present model, in contrast, this 1:1 ratio was obtained by a proper tuning of parameters κ_{1-3} (see section 2.3).

Finally, another important Glu carrier, the electrogenic glutamate-aspartate antiporter AGC1 (Berkich et al., 2007; Das et al., 2022), was not modeled. The coupling of Glu to aspartate transport would withdraw oxaloacetate from the Krebs cycle, and the unidirectionality of AGC1 would not enable Glu to leave. The AGC1 carrier is nevertheless an obligatory component of the (non-modeled) malate-aspartate shuttle (Borst, 2020), which can run in parallel with the present model (see footnote 6).

B.4 Accumulation of glutamate in synaptic vesicles

In glutamatergic boutons, the vesicle membrane contains a proton pump (vacuolar or V-ATPase) and a Glu transporter of the VGLUT family (Dittman & Ryan, 2009; Herzog et al., 2001). The accumulation of Glu is driven by the electrical and pH gradients (inside positive and acid), and hence mediated by an anti-porter (Kolen et al., 2023). Both processes (vesicle acidification and accumulation of Glu) are coupled (Budzinski et al., 2011), and can be modeled by the reaction scheme (Schuldiner et al., 1995):

$$\begin{aligned} 2\mathrm{H}^+_\mathrm{c} + \mathrm{ATP} + \mathrm{H_2O} &\rightarrow 2\mathrm{H}^+_\mathrm{v} + \mathrm{ADP} + \mathrm{P_i} \\ \mathrm{L\text{-}Glutamate_c} + \mathrm{H}^+_\mathrm{v} &\rightarrow \mathrm{L\text{-}glutamate_v} + \mathrm{H}^+_\mathrm{c}. \end{aligned} \tag{B5}$$

The reaction of the V-ATPase is irreversible and has a stoichiometry close to two protons for one ATP molecule (Egashira et al., 2015; Johnson et al., 1982).

Appendix C Generalisation of the model to other neurotransmitters

It is feasible to extend the present mechanism of ATP homeostasis to neurons releasing γ-aminobutyric acid (GABA), as the formation of GABA by decarboxylation of Glu also requires the supply of Gln from astrocytes (Andersen et al., 2021). For neurons releasing acetylcholine, a model can be envisaged based on the supply by astrocytes of its presumed precursor citrate (Dienel, 2019; Westergaard et al., 2017).

Another strategy for keeping the production of ATP proportional to the rate of transmitter release (a proportionality guaranteed for Glu by corollary 1) is to have ATP produced in the reactions that form the neurotransmitter. The inhibitory neurotransmitter glycine (Gly), for instance, is formed in neurons by hydroxy-transmethylation of its precursor L-serine (Ser), an amino acid released by perisynaptic astrocytes. The degradation of Ser to Gly in the neuron's mitochondrion can yield from one to 3.5 molecules of ATP, depending on whether the coenzyme NADH reduced in the process is coupled to oxidative phosphorylation or not (Meiser et al., 2016).

A minimal metabolic model of a glycinergic axon bouton would then read

$$\frac{\mathrm{d}\,[\mathrm{Gly}]}{\mathrm{d}t} = \underbrace{\omega\,\kappa_1\,[\mathrm{Ser}]}_{\text{formation from serine}} - \underbrace{\kappa_2\,[\mathrm{Gly}]\,[\mathrm{ATP}]}_{\text{vesicular accumulation}} \tag{B6}$$

$$\frac{\mathrm{d}\,[\mathrm{ATP}]}{\mathrm{d}t} = \underbrace{n\,\omega\,\kappa_1\,[\mathrm{Ser}]}_{\substack{\text{Ser-Gly conversion}\\ \text{in mitochondria}}} - \underbrace{\frac{\kappa_2}{2}\,[\mathrm{Gly}]\,[\mathrm{ATP}]}_{\text{vesicle acidification}} - \underbrace{w\,[\mathrm{ATP}]}_{\text{work}} - \underbrace{\omega\,\kappa_1\,[\mathrm{Ser}]}_{\text{Ser import}}. \tag{B7}$$

where the coefficient n in the first term of equation B7 denotes the number of ATP molecules produced in the degradation of Ser to Gly. If it is further assumed that [Ser] is

constant at 0.4 mM, then baseline levels of Gly (1 mM) and ATP (1.5 mM) are obtained with $\kappa_1 = \frac{1.5}{2.3}\ \mathrm{s}^{-1}$ and $\kappa_2 = \frac{0.4}{2.3}\ \mathrm{mM}^{-1}\,\mathrm{s}^{-1}$. Hence, ATP homeostasis is faster in this model, as the Krebs cycle does not need to expand or contract first. In agreement with the analysis of section 3.3, a greater fraction of ATP is also spent on Gly-Ser cycling:

$$\frac{0.5\,\kappa_2\,[\mathrm{Gly}]\,[\mathrm{ATP}] + \omega\,\kappa_1[\mathrm{Ser}]}{n\,\omega\,\kappa_1[\mathrm{Ser}]} = \frac{1.5\,\kappa_2\,[\mathrm{Gly}]\,[\mathrm{ATP}]}{n\,\kappa_2\,[\mathrm{Gly}]\,[\mathrm{ATP}]} = \frac{1.5}{n},$$

so that even at the maximal yield of ATP ($n = 3.5$), 43 % of the ATP is used for neurotransmitter cycling.

In addition, most glycinergic neurons corelease Glu or GABA (Wallace & Sabatini, 2023). A model of ATP homeostasis for axons coreleasing Gly and GABA would then read

$$\begin{cases} \dfrac{\mathrm{d}\,[\mathrm{Gly}]}{\mathrm{d}t} = \underbrace{\omega\,\kappa_1\,[\mathrm{Ser}]}_{\text{formation from serine}} - \underbrace{\kappa_2\,[\mathrm{Gly}]\,[\mathrm{ATP}]}_{\substack{\text{vesicular Gly}\\ \text{accumulation}}} \\[2ex] \dfrac{\mathrm{d}\,[\mathrm{GABA}]}{\mathrm{d}t} = \underbrace{\omega\,\kappa_3\,[\mathrm{Gln}]\,[\mathrm{P_i}]^2}_{\text{formation from Gln}} - \underbrace{\kappa_4\,[\mathrm{GABA}]\,[\mathrm{ATP}]}_{\substack{\text{vesicular GABA}\\ \text{accumulation}}} \\[2ex] \dfrac{\mathrm{d}\,[\mathrm{ATP}]}{\mathrm{d}t} = \underbrace{n\,\omega\,\kappa_1\,[\mathrm{Ser}]}_{\substack{\text{Ser-Gly conversion}\\ \text{in mitochondria}}} + \underbrace{\kappa_5\,[\mathrm{Pyr}]\,[\mathrm{GABA}]\left[\dfrac{[\mathrm{P_i}]\,[\mathrm{ADP}]}{[\mathrm{ATP}]}\right]}_{\substack{\text{production via Krebs cycle}\\ \text{in mitochondria}}} - \underbrace{w\,[\mathrm{ATP}]}_{\text{work}} \\ \qquad - \underbrace{\dfrac{\kappa_2}{2}\,[\mathrm{Gly}]\,[\mathrm{ATP}]}_{\substack{\text{vesicular Gly}\\ \text{accumulation}}} - \underbrace{\omega\,\kappa_1\,[\mathrm{Ser}]}_{\text{Ser import}} - \underbrace{\dfrac{\kappa_4}{2}\,[\mathrm{GABA}]\,[\mathrm{ATP}]}_{\substack{\text{vesicular GABA}\\ \text{accumulation}}} - \underbrace{\omega\,\kappa_3\,[\mathrm{Gln}]\,[\mathrm{P_i}]^2}_{\text{Gln import}}. \end{cases}$$

where k_2/k_4 represents the relative affinity of Gly and GABA for the shared vesicular GABA transporter. The steady-state ATP concentration of this system of equations is independent of the workload w. With the additional constraint that $k_2 = 0.4\,k_4$ (Burger

et al., 1991), the free parameters κ_{1-5} can be determined.

The above glycinergic model of ATP homeostasis produces ATP during the *formation* of neurotransmitter. A variant of this model may apply to neurons releasing the monoamines dopamine, NOR-adrenaline or serotonin, in which ATP can be produced by partial *degradation* of the transmitter (Graves et al., 2020). Leakage of vesicular monoamines into the cytosol causes a high intracellular transmitter turnover in these neurons (Eisenhofer, Kopin, & Goldstein, 2004), so that oxidizing part of the transmitter pool may be a strategy for keeping the production of ATP proportional to the rate of monoamine release. The second requirement for ATP homeostasis, that transmitter formation be activity-dependent as well, can be fulfilled by the fast and activity-induced phosphorylation of the enzyme tyrosine (tryptophan) hydroxylase (Zigmond, Schwarzschild, & Rittenhouse, 1989).

Appendix D The role of calcium as hidden variable

The modulation of mitochondrial dehydrogenases by Ca^{2+} ions (Denton & McCormack, 1980), and additional effects of Ca^{2+} on the energy transduction chain (Glancy & Balaban, 2012), indicate a regulatory role for Ca^{2+} in ATP production. Presynaptic mitochondria in particular are sensitive to changes in the cytosolic concentration of Ca^{2+}, which acts as a mediator between the workload and ATP production (Ashrafi, de Juan-Sanz, Farrell, & Ryan, 2020). Although the model does not monitor [Ca^{2+}] as a separate variable, all terms of equations 1 and 2 implicitly depend on cytosolic or mitochondrial [Ca^{2+}]. An increased flux of the Krebs cycle (first term of equation 2), for

instance, may also be obtained by activating the Ca^{2+}-sensitive enzyme α-ketoglutarate dehydrogenase (Cortassa et al., 2003).

There are two special cases then, mathematically, in which a Ca^{2+} dependency may be incorporated in the model without violating theorem 1. In the first case, $[Ca^{2+}]$ would itself be a marker of the workload w. This would require hyperparameter ω to scale with $[Ca^{2+}]$ as well, which is consistent with the observed activation of the PAG enzyme by Ca^{2+} ions in rat brain synaptosomes (Kvamme et al., 2001). In the second special case, not excluding the first, the two terms of equations 1 and 2 explicitly featuring [Glu] (the terms specifying the rates of ATP production and Glu accumulation) would need to have identical Ca^{2+} dependencies, such that [Glu] can be replaced by a stationary function of the form $f([\mathrm{Glu}], [\mathrm{Ca}^{2+}])$, with theorem 1 still holding.

References

Alberty, R. A. (1969). Thermodynamics of the hydrolysis of adenosine triphosphate. *Journal of Chemical Education*, *46*(11), 713–719. 10.1021/ed046p713

Andersen, J. V., Markussen, K. H., Jakobsen, E., Schousboe, A., Waagepetersen, H. S., Rosenberg, P. A., & Aldana, B. I. (2021). Glutamate metabolism and recycling at the excitatory synapse in health and neurodegeneration. *Neuropharmacology*, *196*, 108719. 10.1016/j.neuropharm.2021.108719

Arce-Molina, R., Cortés-Molina, F., Sandoval, P. Y., Galaz, A., Alegría, K., Schirmeier, S., … San Martín, A. (2020). A highly responsive pyruvate sensor reveals pathway-regulatory role of the mitochondrial pyruvate carrier MPC. *Elife*, *9*,

e53917. 10.7554/eLife.53917

Ashrafi, G., de Juan-Sanz, J., Farrell, R. J., & Ryan, T. A. (2020). Molecular tuning of the axonal mitochondrial Ca^{2+} uniporter ensures metabolic flexibility of neurotransmission. *Neuron*, *105*(4), 678–687. 10.1016/j.neuron.2019.11.020

Ashrafi, G., Wu, Z., Farrell, R. J., & Ryan, T. A. (2017). GLUT4 mobilization supports energetic demands of active synapses. *Neuron*, *93*(3), 606–615. 10.1016/j.neuron.2016.12.020

Attwell, D., & Laughlin, S. B. (2001). An energy budget for signaling in the grey matter of the brain. *Journal of Cerebral Blood Flow and Metabolism*, *21*(10), 1133–1145. 10.1097/00004647-200110000-00001

Baytas, O., Davidson, S. M., DeBerardinis, R. J., & Morrow, E. M. (2022). Mitochondrial enzyme GPT2 regulates metabolic mechanisms required for neuron growth and motor function *in vivo*. *Human Molecular Genetics*, *31*(4), 587–603. 10.1093/hmg/ddab269

Beaulieu, C., & Colonnier, M. (1985). A laminar analysis of the number of round-asymmetrical and flat-symmetrical synapses on spines, dendritic trunks, and cell bodies in area 17 of the cat. *Journal of Comparative Neurology*, *231*(2), 180–189. 10.1002/cne.902310206

Bellocchio, E. E., Hu, H., Pohorille, A., Chan, J., Pickel, V. M., & Edwards, R. H. (1998). The localization of the brain-specific inorganic phosphate transporter suggests a specific presynaptic role in glutamatergic transmission. *Journal of Neuroscience*, *18*(21), 8648–8659. 10.1523/JNEUROSCI.18-21-08648.1998

Berkich, D. A., Ola, M. S., Cole, J., Sweatt, A. J., Hutson, S. M., & LaNoue, K. F.

(2007). Mitochondrial transport proteins of the brain. *Journal of Neuroscience Research*, *85*, 3367–3377. 10.1002/jnr.21500

Borst, P. (2020). The malate-aspartate shuttle (Borst cycle): How it started and developed into a major metabolic pathway. *IUBMB Life*, *72*(11), 2241–2259. 10.1002/iub.2367

Brown, G. C. (1992). Control of respiration and ATP synthesis in mammalian mitochondria and cells. *Biochemical Journal*, *284 (Pt 1)*, 1–13. 10.1042/bj2840001

Budzinski, K. L., Zeigler, M., Fujimoto, B. S., Bajjalieh, S. M., & Chiu, D. T. (2011). Measurements of the acidification kinetics of single SynaptopHluorin vesicles. *Biophysical Journal*, *101*(7), 1580–1589. 10.1016/j.bpj.2011.08.032

Burger, P. M., Hell, J., Mehl, E., Krasel, C., Lottspeich, F., & Jahn, R. (1991). GABA and glycine in synaptic vesicles: storage and transport characteristics. *Neuron*, *7*, 287–293. 10.1016/0896-6273(91)90267-4

Cheret, C., Ganzella, M., Preobraschenski, J., Jahn, R., & Ahnert-Hilger, G. (2021). Vesicular glutamate transporters (SLCA17 A6, 7, 8) control synaptic phosphate levels. *Cell Reports*, *34*(2), 108623. 10.1016/j.celrep.2020.108623

Cheung, G., Bataveljic, D., Visser, J., Kumar, N., Moulard, J., Dallérac, G., … Rouach, N. (2022). Physiological synaptic activity and recognition memory require astroglial glutamine. *Nature Communications*, *13*(1), 753. 10.1038/s41467-022-28331-7

Cheung, G., Chever, O., Rollenhagen, A., Quenech'du, N., Ezan, P., Lübke, J. H. R., & Rouach, N. (2023). Astroglial connexin 43 regulates synaptic vesicle release at hippocampal synapses. *Cells*, *12*, 1133. 10.3390/cells12081133

Cooper, A. J., & Jeitner, T. M. (2016). Central role of glutamate metabolism in the maintenance of nitrogen homeostasis in normal and hyperammonemic brain. *Biomolecules*, *6*(2), 16. 10.3390/biom6020016

Cooper, A. J., & Plum, F. (1987). Biochemistry and physiology of brain ammonia. *Physiological Reviews*, *67*, 440–519. 10.1152/physrev.1987.67.2.440

Cortassa, S., Aon, M. A., Marbán, E., Winslow, R. L., & O'Rourke, B. (2003). An integrated model of cardiac mitochondrial energy metabolism and calcium dynamics. *Biophysical Journal*, *84*, 2734–2755. 10.1016/S0006-3495(03)75079-6

Danbolt, N. C. (2001). Glutamate uptake. *Progress in Neurobiology*, *65*(1), 1–105. 10.1016/s0301-0082(00)00067-8

Das, A., Gauthier-Coles, G., Bröer, S., & Rae, C. D. (2022). Impact of inhibition of glutamine and alanine transport on cerebellar glial and neuronal metabolism. *Biomolecules*, *12*(9), 1189. 10.3390/biom12091189

Denton, R. M., & McCormack, J. G. (1980). On the role of the calcium transport cycle in heart and other mammalian mitochondria. *FEBS Letters*, *119*(1), 1–8. 10.1016/0014-5793(80)80986-0

Dienel, G. A. (2019). Brain glucose metabolism: integration of energetics with function. *Physiological Reviews*, *99*(1), 949–1045. 10.1152/physrev.00062.2017

Dittman, J., & Ryan, T. A. (2009). Molecular circuitry of endocytosis at nerve terminals. *Annual Review of Cell and Developmental Biology*, *25*, 133–160. 10.1146/annurev.cellbio.042308.113302

Dobolyi, A., Cservenák, M., Bagó, A. G., Chen, C., Stepanova, A., Paal, K., … Chinopoulos, C. (2024). Cell-specific expression of key mitochondrial enzymes

limits OXPHOS in astrocytes of the adult human neocortex and hippocampal formation. *Communications Biology*, *7*, 1045. 10.1038/s42003-024-06751-z

Egashira, Y., Takase, M., & Takamori, S. (2015). Monitoring of vacuolar-type H^+ ATPase-mediated proton influx into synaptic vesicles. *Journal of Neuroscience*, *35*(8), 3701–3710. 10.1523/JNEUROSCI.4160-14.2015

Eisenhofer, G., Kopin, I. J., & Goldstein, D. S. (2004). Catecholamine metabolism: A contemporary view with implications for physiology and medicine. *Pharmacological Reviews*, *56*(3), 331–349. 10.1124/pr.56.3.1

Engel, P. C., & Dalziel, K. (1967). The equilibrium constants of the glutamate dehydrogenase systems. *Biochemical Journal*, *105*, 691–695. 10.1042/bj1050691

Erecińska, M., & Dagani, F. (1990). Relationships between the neuronal sodium/potassium pump and energy metabolism. Effects of K^+, Na^+, and adenosine triphosphate in isolated brain synaptosomes. *Journal of General Physiology*, *95*(4), 591–616. 10.1085/jgp.95.4.591

Erecińska, M., Nelson, D., & Silver, I. A. (1996). Metabolic and energetic properties of isolated nerve ending particles (synaptosomes). *Biochimica et Biophysica Acta*, *1277*(1–2), 13–34. 10.1016/s0005-2728(96)00103-x

Erecińska, M., & Silver, I. A. (1989). ATP and brain function. *Journal of Cerebral Blood Flow and Metabolism*, *9*(1), 2–19. 10.1038/jcbfm.1989.2

Erecińska, M., & Silver, I. A. (1990). Metabolism and role of glutamate in mammalian brain. *Progress in Neurobiology*, *35*(4), 245–296. 10.1016/0301-0082(90)90013-7

Erickson, J. D., Kyllo, T., & Wulff, H. (2023). Ca^{2+}-regulated expression of high

affinity methylaminoisobutryic acid transport in hippocampal neurons inhibited by riluzole and novel neuroprotective aminothiazoles. *Current Research in Physiology*, *6*, 100109. 10.1016/j.crphys.2023.100109

Ermentrout, B. (2002). *Simulating, Analyzing, and Animating Dynamical Systems*. Philadelphia: SIAM.

Fiermonte, G., Palmieri, L., Todisco, S., Agrimi, G., Palmieri, F., & Walker, J. E. (2002). Identification of the mitochondrial glutamate transporter. Bacterial expression, reconstitution, functional characterization, and tissue distribution of two human isoforms. *Journal of Biological Chemistry*, *277*(22), 19289–19294. 10.1074/jbc.M201572200

Garcia, G. C., Bartol, T. M., Phan, S., Bushong, E. A., Perkins, G., Sejnowski, T. J., ... Skupin, A. (2019). Mitochondrial morphology provides a mechanism for energy buffering at synapses. *Scientific Reports*, *9*, 18306. 10.1038/s41598-019-54159-1

Garcia, G. C., Gupta, K., Bartol, T. M., Sejnowski, T. J., & Rangamani, P. (2023). Mitochondrial morphology governs ATP production rate. *Journal of General Physiology*, *155*, e202213263. 10.1085/jgp.202213263

Ghézali, G., Dallérac, G., & Rouach, N. (2016). Perisynaptic astroglial processes: dynamic processors of neuronal information. *Brain Structure and Function*, *221*(5), 2427–2442. 10.1007/s00429-015-1070-3

Glancy, B., & Balaban, R. S. (2012). Role of mitochondrial Ca^{2+} in the regulation of cellular energetics. *Biochemistry*, *51*(14), 2959–2973. 10.1021/bi2018909

Graves, S. M., Xie, Z., Stout, K. A., Zampese, E., Burbulla, L. F., Shih, J. C., ...

Surmeier, D. J. (2020). Dopamine metabolism by a monoamine oxidase mitochondrial shuttle activates the electron transport chain. *Nature Neuroscience*, *23*, 15–20. 10.1038/s41593-019-0556-3

Hall, C. N., Klein-Flügge, M. C., Howarth, C., & Attwell, D. (2012). Oxidative phosphorylation, not glycolysis, powers presynaptic and postsynaptic mechanisms underlying brain information processing. *Journal of Neuroscience*, *32*(26), 8940–8951. 10.1523/JNEUROSCI.0026-12.2012

Hertz, L. (2004). Intercellular metabolic compartmentation in the brain: past, present and future. *Neurochemistry International*, *45*(2–3), 285–296. 10.1016/j.neuint.2003.08.016

Hertz, L., Dringen, R., Schousboe, A., & Robinson, S. R. (1999). Astrocytes: glutamate producers for neurons. *Journal of Neuroscience Research*, *57*(4), 417–428. 10.1002/(SICI)1097-4547(19990815)57:4¡417::AID-JNR1¿3.0.CO;2-N

Herzog, E., Bellenchi, G. C., Gras, C., Bernard, V., Ravassard, P., Bedet, C., … El Mestikawy, S. (2001). The existence of a second vesicular glutamate transporter specifies subpopulations of glutamatergic neurons. *Journal of Neuroscience*, *21*(22), RC181. 10.1523/JNEUROSCI.21-22-j0001.2001

Hill, T. L. (1989). *Free Energy Transduction and Biochemical Cycle Kinetics*. New York (NY): Springer. 10.1007/978-1-4612-3558-3

Hogstad, S., Svenneby, G., Torgner, I. A., Kvamme, E., Hertz, L., & Schousboe, A. (1988). Glutaminase in neurons and astrocytes cultured from mouse brain: kinetic properties and effects of phosphate, glutamate, and ammonia. *Neurochemical Research*, *13*, 383–388. 10.1007/BF00972489

Hohnholt, M. C., Andersen, V. H., Andersen, J. V., Christensen, S. K., Karaca, M., Maechler, P., & Waagepetersen, H. S. (2018). Glutamate dehydrogenase is essential to sustain neuronal oxidative energy metabolism during stimulation. *Journal of Cerebral Blood Flow and Metabolism*, *38*(10), 1754–1768. 10.1177/0271678X17714680

Hori, T., & Takahashi, T. (2012). Kinetics of synaptic vesicle refilling with neurotransmitter glutamate. *Neuron*, *76*, 511–517. 10.1016/j.neuron.2012.08.013

Howarth, C., Gleeson, P., & Attwell, D. (2012). Updated energy budgets for neural computation in the neocortex and cerebellum. *Journal of Cerebral Blood Flow and Metabolism*, *32*, 1222–1232. 10.1038/jcbfm.2012.35

Ishikawa, T., Sahara, Y., & Takahashi, T. (2002). A single packet of transmitter does not saturate postsynaptic glutamate receptors. *Neuron*, *34*(4), 613–621. 10.1016/s0896-6273(02)00692-x

Jeneson, J. A., Westerhoff, H. V., Brown, T. R., Van Echteld, C. J., & Berger, R. (1995). Quasi-linear relationship between Gibbs free energy of ATP hydrolysis and power output in human forearm muscle. *American Journal of Physiology*, *268*, C1474–C1484. 10.1152/ajpcell.1995.268.6.C1474

Jiang, L., Shestov, A. A., Swain, P., Yang, C., Parker, S. J., Wang, Q. A., ... DeBerardinis, R. J. (2016). Reductive carboxylation supports redox homeostasis during anchorage-independent growth. *Nature*, *532*, 255–258. 10.1038/nature17393

Johnson, R. G., Beers, M. F., & Scarpa, A. (1982). H^+ ATPase of chromaffin granules. Kinetics, regulation, and stoichiometry. *Journal of Biological Chemistry*, *257*(18), 10701–10707. 10.1016/S0021-9258(18)33879-1

Juhaszova, M., Kobrinsky, E., Zorov, D. B., Nuss, H. B., Yaniv, Y., Fishbein, K. W., ... Sollott, S. J. (2021). ATP synthase K^+ and H^+-fluxes drive ATP synthesis and enable mitochondrial K^+-"uniporter" function: I. Characterization of ion fluxes. *Function (Oxford, England)*, *3*, zqab065. 10.1093/function/zqab065

Kolen, B., Borghans, B., Kortzak, D., Lugo, V., Hannack, C., Guzman, R. E., ... Fahlke, C. (2023). Vesicular glutamate transporters are H^+-anion exchangers that operate at variable stoichiometry. *Nature Communications*, *14*(1), 2723. 10.1038/s41467-023-38340-9

Krebs, H. A. (1953). *The citric acid cycle.* Retrieved from `nobelprize.org/prizes/medicine/1953/krebs/lecture`

Krebs, H. A. (1970). Rate control of the tricarboxylic acid cycle. *Advances in Enzyme Regulation*, *8*, 335–353. 10.1016/0065-2571(70)90028-2

Kvamme, E., Torgner, I. A., & Roberg, B. (2001). Kinetics and localization of brain phosphate activated glutaminase. *Journal of Neuroscience Research*, *66*(5), 951–958. 10.1002/jnr.10041

Lennie, P. (2003). The cost of cortical computation. *Current Biology*, *13*, 493–497. 10.1016/s0960-9822(03)00135-0

Li, B., & Freeman, R. D. (2015). Neurometabolic coupling between neural activity, glucose, and lactate in activated visual cortex. *Journal of Neurochemistry*, *135*, 742–754. 10.1111/jnc.13143

Lieth, E., LaNoue, K. F., Berkich, D. A., Xu, B., Ratz, M., Taylor, C., & Hutson, S. M. (2001). Nitrogen shuttling between neurons and glial cells during glutamate synthesis. *Journal of Neurochemistry*, *76*(6), 1712–1723. 10.1046/j.1471-

4159.2001.00156.x

Magi, S., Arcangeli, S., Castaldo, P., Nasti, A. A., Berrino, L., Piegari, E., ... Lariccia, V. (2013). Glutamate-induced ATP synthesis: relationship between plasma membrane Na^+/Ca^{2+} exchanger and excitatory amino acid transporters in brain and heart cell models. *Molecular Pharmacology*, *84*(4), 603–614. 10.1124/mol.113.087775

Magnus, G., & Keizer, J. (1997). Minimal model of β-cell mitochondrial Ca^{2+} handling. *American Journal of Physiology*, *273*, C717–C733. 10.1152/ajpcell.1997.273.2.C717

Mangia, S., Giove, F., & Dinuzzo, M. (2012). Metabolic pathways and activity-dependent modulation of glutamate concentration in the human brain. *Neurochemical Research*, *37*(11), 2554–2561. 10.1007/s11064-012-0848-4

Marx, M. C., Billups, D., & Billups, B. (2015). Maintaining the presynaptic glutamate supply for excitatory neurotransmission. *Journal of Neuroscience Research*, *93*(7), 1031–1044. 10.1002/jnr.23561

Mason, G. F., Gruetter, R., Rothman, D. L., Behar, K. L., Shulman, R. G., & Novotny, E. J. (1995). Simultaneous determination of the rates of the TCA cycle, glucose utilization, α-ketoglutarate/glutamate exchange, and glutamine synthesis in human brain by NMR. *Journal of Cerebral Blood Flow and Metabolism*, *15*(1), 12–25. 10.1038/jcbfm.1995.2

Meiser, J., Tumanov, S., Maddocks, O., Labuschagne, C. F., Athineos, D., Van Den Broek, N., ... Vazquez, A. (2016). Serine one-carbon catabolism with formate overflow. *Science Advances*, *2*, e1601273. 10.1126/sciadv.1601273

Nelson, D. L., & Cox, M. M. (2013). *Lehninger Principles of Biochemistry*. New York: W. H. Freeman.

Nicholls, D. G., & Ferguson, S. J. (2002). *Bioenergetics* (3rd ed.). London (UK): Academic Press.

Nicholls, D. G., Grav, H. J., & Lindberg, O. (1972). Mitochondria from hamster brown-adipose tissue. Regulation of respiration *in vitro* by variations in volume of the matrix compartment. *European Journal of Biochemistry*, *31*, 526–533. 10.1111/j.1432-1033.1972.tb02561.x

Ouyang, Q., Nakayama, T., Baytas, O., Davidson, S. M., Yang, C., Schmidt, M., … Morrow, E. M. (2016). Mutations in mitochondrial enzyme GPT2 cause metabolic dysfunction and neurological disease with developmental and progressive features. *Proceedings of the National Academy of Sciences*, *113*(38), E5598–E5607. 10.1073/pnas.1609221113

Peca, S., , M., Di Bonaventura, C., Aprile, T., Hagberg, G. E., Giallonardo, A. T., … Giove, F. (2010). Metabolic correlatives of brain activity in a FOS epilepsy patient. *NMR in Biomedicine*, *23*(2), 170–178. 10.1002/nbm.1439

Pulido, C., & Ryan, T. A. (2021). Synaptic vesicle pools are a major hidden resting metabolic burden of nerve terminals. *Science Advances*, *7*(49), eabi9027. 10.1126/sciadv.abi9027

Rae, C. D., Baur, J. A., Borges, K., Dienel, G., Díaz-García, C. M., Douglass, S. R., … McKenna, M. C. (2024). Brain energy metabolism: A roadmap for future research. *Journal of Neurochemistry*, *168*(5), 910–954. 10.1111/jnc.16032

Rangaraju, V., Calloway, N., & Ryan, T. A. (2014). Activity-driven local

ATP synthesis is required for synaptic function. *Cell*, *156*(4), 825–835. 10.1016/j.cell.2013.12.042

Rothman, D. L., Behar, K. L., & Dienel, G. A. (2024). Mechanistic stoichiometric relationship between the rates of neurotransmission and neuronal glucose oxidation: Reevaluation of and alternatives to the pseudo-malate-aspartate shuttle model. *Journal of Neurochemistry*, *168*(5), 555–591. 10.1111/jnc.15619

Sauter, A., & Rudin, M. (1993). Determination of creatine kinase kinetic parameters in rat brain by NMR magnetization transfer. Correlation with brain function. *Journal of Biological Chemistry*, *268*, 13166–13171. 10.1016/S0021-9258(19)38633-8

Schuldiner, S., Shirvan, A., & Linial, M. (1995). Vesicular neurotransmitter transporters: from bacteria to humans. *Physiological Reviews*, *75*(2), 369–392. 10.1152/physrev.1995.75.2.369

Segel, L. A. (1984). *Modeling Dynamic Phenomena in Molecular and Cellular Biology*. Cambridge (UK): Cambridge University Press.

Shepherd, G. M., & Harris, K. M. (1998). CA1 axons in rat hippocampal slices: implications for presynaptic connectivity and compartmentalization. *Journal of Neuroscience*, *18*(20), 8300–8310. 10.1523/JNEUROSCI.18-20-08300.1998

Sibson, N. R., Dhankhar, A., Mason, G. F., Rothman, D. L., Behar, K. L., & Shulman, R. G. (1998). Stoichiometric coupling of brain glucose metabolism and glutamatergic neuronal activity. *Proceedings of the National Academy of Sciences*, *95*(1), 316–321. 10.1073/pnas.95.1.316

Stern, A., Fokra, M., Sarvin, B., Alrahem, A. A., Lee, W. D., Aizenshtein, E., …

Shlomi, T. (2023). Inferring mitochondrial and cytosolic metabolism by coupling isotope tracing and deconvolution. *Nature Communications*, *14*(1), 7525. 10.1038/s41467-023-42824-z

Tani, H., Dulla, C. G., Farzampour, Z., Taylor-Weiner, A., Huguenard, J. R., & Reimer, R. J. (2014). A local glutamate-glutamine cycle sustains synaptic excitatory transmitter release. *Neuron*, *81*(4), 888–900. 10.1016/j.neuron.2013.12.026

Tveit, B., Svenneby, G., & Kvamme, E. (1970). Kinetic properties of glutaminase from pig renal cortex. *European Journal of Biochemistry*, *14*(2), 337–344. 10.1111/j.1432-1033.1970.tb00294.x

Varoqui, H., Zhu, H., Yao, D., Ming, H., & Erickson, J. D. (2000). Cloning and functional identification of a neuronal glutamine transporter. *Journal of Biological Chemistry*, *275*(6), 4049–4054. 10.1074/jbc.275.6.4049

Vaupel, P., & Multhoff, G. (2021). Revisiting the Warburg effect: historical dogma versus current understanding. *Journal of Physiology*, *599*(6), 1745–1757. 10.1113/JP278810

Wallace, M. L., & Sabatini, B. L. (2023). Synaptic and circuit functions of multitransmitter neurons in the mammalian brain. *Neuron*, *111*(19), 2969–2983. 10.1016/j.neuron.2023.06.003

Wang, Y., Fathali, H., Mishra, D., Olsson, T., Keighron, J. D., Skibicka, K. P., & Cans, A. S. (2019). Counting the number of glutamate molecules in single synaptic vesicles. *Journal of the American Chemical Society*, *141*(44), 17507–17511. 10.1021/jacs.9b09414

Westergaard, N., Waagepetersen, H. S., Belhage, B., & Schousboe, A. (2017). Citrate,

a ubiquitous key metabolite with regulatory function in the CNS. *Neurochemical Research*, *42*(6), 1583–1588. 10.1007/s11064-016-2159-7

Wiehler, A., Branzoli, F., Adanyeguh, I., Mochel, F., & Pessiglione, M. (2022). A neuro-metabolic account of why daylong cognitive work alters the control of economic decisions. *Current Biology*, *32*(16), 3564–3575. 10.1016/j.cub.2022.07.010

Yu, Y., Herman, P., Rothman, D. L., Agarwal, D., & Hyder, F. (2018). Evaluating the gray and white matter energy budgets of human brain function. *Journal of Cerebral Blood Flow and Metabolism*, *38*(8), 1339–1353. 10.1177/0271678X17708691

Zigmond, R. E., Schwarzschild, M. A., & Rittenhouse, A. R. (1989). Acute regulation of tyrosine hydroxylase by nerve activity and by neurotransmitters via phosphorylation. *Annual Review of Neuroscience*, *12*, 415–461. 10.1146/annurev.ne.12.030189.002215